"Evolution of 231Pa and 230Th in overflow waters of the North Atlantic"
by Feifei Deng et al.

Response to referees

We would like to thank all referees for their time reading the revised manuscript and giving constructive suggestions to further improve the paper. We are pleased that the referees appreciate our clarification and revision of the initial manuscript, and give favourable reports for the paper.

Below, we respond to the referees according to report 1 point by point. Reviewer's comments from report 1 are in blue, and our responses are in black.

Report 1:

Deng et al. have provided a thoughtful response to comments from the referees, and the authors have made helpful clarifications in revising their text. I recommend publication with just a few further changes.

The following comments refer to page and line numbers in the authors' response version of the revised manuscript.

1) Section 4.3, p. 8, around line 29: Although the model equation from Moran et al. (1997) is given in the Supplementary Material, it would be easier for readers to understand the findings described in the text if the model equation were included in the main text. It was not immediately obvious to me how the model curves in Figure 9 were obtained until I realized that the curves were derived by plugging the preformed concentrations, S, SPM and Kd into Moran's equation (originally from Rutgers van der Loeff?) along with the reference depth (either 2000 m or 3500 m) to obtain the curves as a function of water mass age. Anticipating that other readers may similarly find this hard to follow, I recommend that the equation be added to the main text so that readers can see immediately how the curves in Figure 9 were obtained.

Author's response:
Thank you for pointing this out. As suggested, we have added a brief description of the equation from Moran et al. (1997) in the main text, and have kept a detailed version of the description of the model and parameterization in the SI.

2) p. 9, lines 11-14: It is not only possible that scavenging of 230Th is more intense than would be inferred from the parameters derived using Station 13 data, the model-data offsets observed here require this. I suggest adding a sentence or two to speculate about why scavenging may be greater than at Station 13 at these locations.

Author's response:
Thank you for pointing this out. In the last revised manuscript, we suggested additional scavenging close to the seafloor in LA and IR Seas for deep water as a possible cause of the model-data offsets. But, we would add a sentence on p.9, line 23 to indicate the possibility of differences in productivity between stations causing some changes in scavenging as another cause.

3) p. 9, line 27: Delete “from” in “those in from DSOW”

Author’s response:
The text in the last revised manuscript was “…, particularly those from DSOW in the deepest LA Sea”. We do not see the gramma issue here, and have kept the text as it was.

4) Figure 6, caption, change “older waters west of” to “older waters east of”

Author’s response:
Thank you for correcting. We have made the correction as suggested.

5) Figure 7, bottom left panel, in the heading change “Observed” to “Scavenged”

Author’s response:
Thank you for spotting the mistake. We have corrected the mistake as suggested.

6) Figure S1, caption, change “profiles of and 13” to “profiles of Station 13”

Author’s response:
Thank you for spotting the typo. We have corrected as suggested. We have also made it consistent by capitalizing S in the word station. This change is made in p10, line 10 in SI.

7) Section S4, providing information about sources of uncertainty in the assessment of scavenging, is very important. I recommend moving it to the Discussion section of the main text.

Author’s response:
Thank you for your suggestion. We agree with the reviewer and have moved this information to the main text as a new short Section 4.5 in the discussion section of the main text. The sentence on p. 9, line 24 in the last revised manuscript indicating such information was in SI has been removed. Section 4.5 in the last revised manuscript is therefore renumbered as section 4.6. Accordingly, this information has been removed entirely from SI, and Supplemental Information S5 is renumbered as S4, and where it is referred is also corrected (p11, line 9 in this revised manuscript).

8) Supplementary material, the Journal, Volume and page numbers is missing for the first reference.

Author’s response:
Thank you for pointing out. We have made the correction.

Summary: As stated in my original review, the authors present a valuable new data set. The discussion of the sensitivity of Pa/Th ratios to preformed (initial) dissolved 231Pa and 230Th concentrations, to my knowledge, has not been presented before. This is a particularly useful discussion to help direct future studies of the Pa/Th ratio as a paleo circulation proxy when applied to North Atlantic sediments.

Evolution of ^{231}Pa and ^{230}Th in overflow waters of the North Atlantic

Feifei Deng[1], Gideon M. Henderson[1], Maxi Castrillejo[2,3], Fiz F. Perez[4] and Reiner Steinfeldt[5]

[1]Department of Earth Sciences, University of Oxford, South Parks Road, Oxford, OX13AN, UK.

[2]LaboraLaboratory of Ion Beam Physics, ETH-Zurich, Otto Stern Weg 5, Zurich, 8093, Switzerland.

[3]Institut de Ciència i Tecnologia Ambientals & Departament de Física, Universitat Autònoma de Barcelona, Bellaterra, 08193, Spain.

[4]Departamento de Oceanografia Instituto Investigaciones Marinas (CSIC), Eduardo Cabello 6, E36208 Vigo, Spain.

[5]Institut fur Umweltphysik, Universitat Bremen, D-28334 Bremen, Germany.

Correspondence to: Feifei Deng (feifei.deng@earth.ox.ac.uk)

Abstract. Many paleoceanographic studies have sought to use the ^{231}Pa/^{230}Th ratio as a proxy for deep ocean circulation rates in the North Atlantic. As yet, however, no study has fully assessed the concentration of, or controls on, ^{230}Th and ^{231}Pa in waters immediately following ventilation at the start of Atlantic meridional overturning. To that end, full water-column ^{231}Pa and ^{230}Th concentrations were measured along the GEOVIDE section, sampling a range of young North Atlantic deep waters. Th-230 and ^{231}Pa concentrations in the water column are lower than those observed further south in the Atlantic, ranging between 0.06 and 12.01 μBq/kg, and between 0.37 and 4.80 μBq/kg, respectively. Both ^{230}Th and ^{231}Pa profiles generally increase with water depth from surface to deep water, followed by decrease near the seafloor, with this feature most pronounced in the Labrador Sea (LA Sea) and Irminger Sea (IR Sea). Assessing this dataset using Extended Optimum Multi-Parameter (eOMP) analysis and CFC-based water mass age indicates that the low values of ^{230}Th and ^{231}Pa in water near the seafloor of the LA Sea and IR Sea are related to the young waters present in those regions. The importance of water age is confirmed for ^{230}Th by a strong correlation between ^{230}Th and water mass age (though this relationship with age is less clear for ^{231}Pa and the ^{231}Pa/^{230}Th ratio). Scavenged ^{231}Pa and ^{230}Th were estimated and compared to their potential concentrations in the water column due to ingrowth. This calculation indicates that more ^{230}Th is scavenged (~80%) than ^{231}Pa (~40%), consistent with the relatively higher particle-reactivity of ^{230}Th. Enhanced scavenging for both nuclides is demonstrated near the seafloor in young overflow waters. Calculation of meridional transport of ^{230}Th and ^{231}Pa with this new GEOVIDE dataset enables a complete budget for ^{230}Th and ^{231}Pa for the North Atlantic. Results suggest that net transport southward of ^{230}Th and ^{231}Pa across GEOVIDE is smaller than transport further south in the Atlantic, and indicates that the flux to sediment in the North Atlantic is equivalent to 96% of the production of ^{230}Th, and 74% of the production for ^{231}Pa. This result confirms a significantly higher advective loss of ^{231}Pa to the south relative to ^{230}Th and supports the use of ^{231}Pa/^{230}Th to assess meridional transport at a basin scale.

Key words. GEOTRACES; water-column ^{230}Th and ^{231}Pa; water mass ageing; scavenging; meridional transport.

1 Introduction

Several paleoceanographic proxies have been proposed that rely on the $^{231}Pa/^{230}Th$ ratio in marine sediments, one of which is that $^{231}Pa/^{230}Th$ may record the rate of deep-water circulation, particularly in the North Atlantic. Both ^{231}Pa and ^{230}Th are produced in seawater at a constant rate by decay of uranium, but have decay activities much lower than their parent uranium isotopes due to rapid removal by adsorption onto sinking marine particles. Both nuclides are also reversibly scavenged, leading to particularly low concentrations at the surface and increasing concentrations with depth (Nozaki et al., 1981). Advection of surface waters to depth transports water with low concentrations of ^{231}Pa and ^{230}Th into the deep ocean, where their concentrations subsequently increase towards an equilibrium value at a rate dependant on the residence time of the nuclide. The longer residence time of ^{231}Pa relative to ^{230}Th (~130 years versus ~20 years, Henderson and Anderson, 2003) means that the equilibrium concentration of ^{231}Pa is closer to that expected from uranium decay, and that the time taken to reach this equilibrium is longer.

This oceanic behaviour of ^{231}Pa and ^{230}Th suggests that their measurement in marine sediments may reveal information about the past environment, with one common use being as a recorder of deep-water circulation, particularly in the North Atlantic (e.g. Gherardi et al., 2005, 2009; McManus et al., 2004; Roberts et al., 2014; Yu et al., 1996). The interpretation of sedimentary $^{231}Pa/^{230}Th$ ratios for such past ocean circulation is based on two end-member conceptual models:

Basin-scale Advection: The longer residence time of ^{231}Pa than ^{230}Th means that deep-water contains more ^{231}Pa than ^{230}Th relative to production from decay. Advection of deep-waters out of the North Atlantic therefore removes more ^{231}Pa than ^{230}Th, leaving sediments in the basin with a $^{231}Pa/^{230}Th$ ratio below the production ratio. If deep-water ventilation ceased, ^{231}Pa removal from the North Atlantic also ceases, and sedimentary $^{231}Pa/^{230}Th$ values reach their production ratio. This approach was first proposed by Yu et al. (1996) who measured $^{231}Pa/^{230}Th$ in Holocene and Last Glacial Maximum (LGM) sediments from many core-top samples from the Atlantic and Southern Ocean. They found similar Holocene and LGM values at a basin scale, suggesting broadly similar overturning during the two periods. Subsequent application to sediments from Heinrich Stadial 1, initially in a single core (McManus et al., 2004) and progressively a geographical range of cores (Bradtmiller et al., 2014), revealed reduced advection of ^{231}Pa out of the basin at that time, suggesting decreased overturning.

Water-mass Evolution: The longer residence time of ^{231}Pa means that, following ventilation, it takes longer for deep-water ^{231}Pa concentrations to reach equilibrium with respect to scavenging than is the case for ^{230}Th. This leads to a systematic evolution of $^{231}Pa/^{230}Th$ with age of the water. Sediments capture this ratio (with a fractionation due to different scavenging coefficients for the two nuclides), so capture information about the age of the water. Simple models suggest an increase of $^{231}Pa/^{230}Th$ with age over about 400 years (e.g. several residence times of ^{231}Pa). This approach to interpreting sedimentary $^{231}Pa/^{230}Th$ allows for the possibility of calculating flow rates for a single water mass and from a single core rather than at a basin scale. It has been pursued by (Negre et al., 2010) to assess deep-water flow in both southerly and northerly directions by comparing sediments in the North and South Atlantic, and allowed these authors to apply a simple model (Thomas et al., 2007) to calculate flow rates.

Recent water-column measurements of ^{231}Pa and ^{230}Th on GEOTRACES cruises shed new light on the chemical behaviour and controls on these isotopes in seawater and provided evidence to assess the validity of the models underlying the use of sedimentary ^{231}Pa/^{230}Th as a proxy for deep-water circulation. These measurements have indicated that there is considerably more net advection of ^{231}Pa than ^{230}Th out of the North Atlantic (Deng et al., 2014), supporting the Basin-scale Advection model for ^{231}Pa/^{230}Th. But these measurements also suggest that there is no simple relationship between increasing ^{231}Pa/^{230}Th and age of water, as would be expected for the Water-mass Evolution model (e.g. Deng et al., 2014). Studies using 2-D and 3-D ocean models (e.g. Marchal et al., 2010; Siddall et al., 2007) have also supported the use of sedimentary ^{231}Pa/^{230}Th to constrain deep-water circulation at a basin scale, and suggested that the relationship between ^{231}Pa/^{230}Th and water mass age is more complex than assumed in earlier studies (e.g. Luo et al., 2010).

Observations and model studies of ^{231}Pa and ^{230}Th have also suggested that other controls complicate ^{231}Pa/^{230}Th as a dynamic tracer of deep-water circulation, such as the effect of boundary scavenging at seafloor and ocean margins (e.g. Anderson et al., 1994; Deng et al., 2014; Rempfer et al., 2017) and the influence of particle flux and composition (e.g. Chase et al., 2002; Hayes et al., 2014; Siddall et al., 2005).

To fully assess the behaviour of ^{231}Pa/^{230}Th, and its potential as a dynamic tracer of deep-water circulation, knowledge of the concentrations and variations of these isotopes as deep waters form and enter the deep Atlantic is required. Some measurements have placed initial constraints on ^{231}Pa and ^{230}Th values in young North Atlantic deep waters (e.g. Moran et al., 1997, 2002; Rutgers van der Loeff and Berger, 1993), but there has not yet been a systematic study of the composition of waters in the far north Atlantic. The GEOVIDE cruise allowed waters to be collected for such a study, along a line where significant other data are available, both from that cruise and previous occupations of OVIDE. GEOVIDE provided an ideal opportunity to understand ^{231}Pa and ^{230}Th at the start of the ocean meridional overturning circulation, and to assess the hypotheses underlying the use of ^{231}Pa/^{230}Th as a paleo-proxy for the rate of deep-water circulation.

2 Sampling strategies and analytical methods

Seawater samples were collected during the GEOVIDE cruise aboard the R/V Pourquoi Pas? from 15 May to 30 June, 2014 as part of GEOTRACES Section GA01. The cruise sampled four regions in the North Atlantic between 40º-60ºN: Labrador Sea (LA Sea), Irminger Sea (IR Sea), Iceland Basin (IC Basin), and Western European Basin (WE Basin) (Fig. 1).

Full-depth water-column ^{231}Pa and ^{230}Th for this study were collected from 11 stations (Fig. 1). Sampling followed the procedure suggested by GEOTRACES intercalibration work (Anderson et al., 2012). Briefly, seawater samples of 5 Litres were directly filtered from Niskin bottles mounted on the Stainless Steel CTD Rosette through AcroPak™ capsules with Supor® Membrane (0.45 µm pore size). Filtered seawater samples were collected into acid cleaned HDPE plastic bottles, and sealed with a screw cap and Parafilm to reduce evaporation and contamination. Samples were then double bagged for storage in boxes for transport back to the shore-based lab for analysis.

Once returned to the laboratory in Oxford, samples were weighed and then acidified with quartz distilled concentrated HCl to pH ~1.7, shaken and left for at least four days to ensure that Pa and Th was desorbed from the walls of the bottle. A mixed ^{229}Th-^{236}U spike and a ^{233}Pa spike were then added to each sample to allow measurement of Th, U (for another study), and Pa by isotope dilution MC-ICP-MS (Multi Collector-Inductively Coupled Plasma-Mass Spectrometry). The ^{233}Pa spike was freshly made by milking from ^{237}Np (following Regelous et al., 2004) and calibrated against a known ^{236}U solution after complete decay of ^{233}Pa to ^{233}U, i.e. four to five half-lives of ^{233}Pa ($t_{1/2}$=26.98 days, Usman and MacMahon, 2000) after spike production (Robinson et al., 2004). 50 mg of pure Fe as a chloride solution was also added to each water sample. Samples were left overnight to allow for spike equilibrium after which the pH was raised to ~8.5 using distilled NH_4OH to co-precipitate the actinides with insoluble Fe-oxyhydroxides. At least 48 hours were allowed for scavenging of the actinides onto Fe-oxyhydroxides. The precipitate was centrifuged and rinsed, and Th, Pa and U were separated using anion exchange chromatography following Thomas et al. (2006).

After chemical separation, Pa and Th were measured on a Nu instrument MC-ICP-MS at the University of Oxford. Mass discrimination and ion-counter gain were assessed with the measurement of a U standard, CRM-145 U, before each sample measurement. Use of a U standard for this purpose minimises memory problems that might be caused by use of a Th or Pa standard (Thomas et al., 2006). Measurements were also made 0.5 mass units either side of masses of interest to allow accurate correction for the effect of abundance sensitivity on small ^{231}Pa and ^{230}Th beams, and a correction for a small ^{232}ThH interference on the ^{233}Pa beam is made from assessment of the hydride formation rate on a ^{232}Th standard. Concentrations of ^{231}Pa, ^{230}Th together with ^{232}Th were obtained from the precise MC-ICP-MS measurement of ^{231}Pa/^{233}Pa, ^{230}Th/^{229}Th, and ^{232}Th/^{229}Th ratios together with well-calibrated concentrations of ^{233}Pa, and ^{229}Th-^{236}U spikes.

Chemistry blanks were assessed by conducting the complete chemical procedure on ~100 ml of Milli-Q water with each batch of samples. Based on six blank measurements, the average blanks for dissolved ^{231}Pa, ^{230}Th and ^{232}Th are 0.21±0.14 fg, 1.59±0.60 fg and 5.13±1.47 pg, respectively (uncertainties are 2 standard errors). Blank contributions account for 2-22%, 2-26%, and 0.2-16% of the dissolved ^{231}Pa, ^{230}Th and ^{232}Th respectively (with the higher values being for surface samples due to their low concentrations).

3 Results

Measured ^{230}Th and ^{231}Pa concentrations were corrected for blanks, ingrowth from U in seawater since the time of sample collection, and detrital U-supported ^{230}Th and ^{231}Pa concentrations. Measured and corrected concentrations of ^{230}Th, ^{231}Pa, and ^{232}Th, along with details of corrections, are provided in the Supplemental Information S1. Although analysis was conducted in terms of fg/kg, results are converted to the SI units adopted by GEOTRACES data product, i.e., µBq/kg for ^{230}Th and ^{231}Pa, and pmol/kg for ^{232}Th. This conversion uses half-lives for ^{231}Pa, ^{230}Th and ^{232}Th of 32,760 yr, 75,584 yr and 1.405×10^{10} yr, respectively (Cheng et al., 2013; Holden, 1990; Robert et al., 1969). Uncertainties were propagated, including the contribution from sample weighing, spike calibration, impurities in the spikes, blank corrections, and mass spectrometric measurement,

and are reported as 2 standard errors (2 s.e.). Average total uncertainties for ^{231}Pa, ^{230}Th and ^{232}Th are ±0.17 µBq/kg, ±0.17 µBq/kg, and ±0.0032 pmol/kg, respectively. Vertical profiles showing the results of corrected ^{230}Th and ^{231}Pa concentrations in the water column are plotted by region in Fig. 2.

Th-230 concentrations in the water column range between 0.06 and 12.01 µBq/kg, and initially generally increase with water depth from surface to deep water. Towards the seafloor, six of the eleven stations show a prominent decrease of ^{230}Th, with this feature most pronounced in the LA and IR Seas.

Pa-231 concentrations in the water column range between 0.37 and 4.80 µBq/kg and also increase with water depth, but less rapidly than ^{230}Th. ^{231}Pa profiles also often exhibit a decrease near the seafloor at stations showing a ^{230}Th decrease. Station 38 at the Reykjanes Ridge distinguishes itself from other ^{231}Pa profiles in that an increase in ^{231}Pa concentrations from low concentrations at 1000 m is observed, continuing towards the bottom.

Observed ^{230}Th and ^{231}Pa values at GEOVIDE are lower than those observed in inter-calibrated GEOTRACES data from further south in the Atlantic. Figure 3 compares average depth profiles for ^{230}Th and ^{231}Pa in the west Atlantic, covering high-latitude Northwest Atlantic (from GEOVIDE, west of the Mid-Atlantic Ridge), mid-latitude Northwest Atlantic (GEOTRACES section GA03_w, Hayes et al., 2015) and Southwest Atlantic (GEOTRACES section GA02, Deng et al., 2014). A southward increase of both ^{230}Th and ^{231}Pa concentrations is observed below 1000 m.

4 Discussion

Early studies of water-column ^{230}Th and ^{231}Pa reported a linear increase of both nuclides with water depth (e.g., Anderson et al., 1983b; Nozaki et al., 1981), and introduced a reversible scavenging model with exchange of both nuclides between their dissolved and particulate phases. Later studies observed a deviation of ^{230}Th and ^{231}Pa profiles from this reversible scavenging model, with the expected increase with depth often inverting near the seafloor (e.g., Anderson et al., 1983a; Bacon and Anderson, 1982). This feature has been further investigated in more recent studies. Rutgers van der Loeff and Berger (1993) observed that ^{230}Th concentrations decrease in the bottom water in the South Atlantic south of the Antarctic Polar Front and interpreted this as the influence of relatively young bottom water in the region. Okubo et al. (2012) also found decreasing ^{230}Th values near the seafloor in the North Pacific and, in the absence of ventilation in the area, interpreted these as due to bottom scavenging. Deng et al. (2014) observed low concentrations of both ^{230}Th and ^{231}Pa in near-bottom water coinciding with the presence of the nepheloid layer, and interpreted the low values as a result of enhanced scavenging by resuspended particles in the nepheloid layer.

In this study, recently ventilated overflow waters are sampled at depth, particularly in the Labrador and Irminger Seas. Low values of ^{230}Th and ^{231}Pa near the seafloor might be expected to relate to these young waters, but the effects of scavenging must also be considered.

4.1 Water mass distribution and influence

The presence of multiple water masses sampled by the GEOVIDE Section allows the influence of water mass (and age) on ^{230}Th and ^{231}Pa to be assessed. Extended Optimum Multi-Parameter (eOMP) Analysis (García-Ibáñez et al., 2018) for the GEOVIDE section maps the presence of 10 water-mass end-members in the section (Fig. 4), including three recently ventilated waters in the GEOVIDE section:

i. Labrador Sea Water (LSW), which is formed by deep convection (Talley and McCartney, 1982), is the dominant deep water along the section, extending from 1000 to 2500 m depth in the east and from surface to 3500 m in the west of the section.

ii. Iceland–Scotland Overflow Water (ISOW), which is formed in the Norwegian Sea and subsequently entrains overlying warmer and more salty waters. This water mass initially flows along the eastern flank of the Reykjanes Ridge before spreading back northwards, after crossing the Charlie-Gibbs Fracture Zone, into the Irminger and Labrador Seas (Dickson and Brown, 1994; Saunders, 2001). A pronounced layer of this water mass is observed immediately below the LSW, and extends as deep as 4000 m west of 20ºW.

iii. Denmark Strait Overflow Water (DSOW), which is formed after the Nordic Seas deep waters overflow and entrains Atlantic waters (SPMW and LSW) (Yashayaev and Dickson, 2008) with dense Greenland shelf water cascading down to the DSOW layer in the Irminger Sea (Falina et al., 2012; Olsson et al., 2005; Tanhua et al., 2005). This water occupies the deepest part of the IR and LA Seas.

In the east of the section, deep waters consist of the much older Lower North East Atlantic Deep Water ($NEADW_L$) which is formed with a significant southern component from Antarctic Bottom Water. A number of other water masses are also observed at shallow depths, including Mediterranean Water, and various mode waters.

Some control of water mass on ^{230}Th and ^{231}Pa concentration is evident in nuclide section plots (Fig. 5), particularly relatively low ^{230}Th and ^{231}Pa concentrations in DSOW and high values in the old NEADW. In other places, the impact of water mass is less apparent. The challenge with these nuclides is that they are not conservative tracers of water mass, but evolve significantly during transport and water aging. On the GEOVIDE Section we can analyse this evolution because the ages of the water-masses can be assessed from CFC data.

CFC measurements are not available from the GEOVIDE cruise itself. de la Paz et al. (2017), however, measured CFC concentrations along the west of the same section (covering WE Basin, IC Basin, and IR Sea) in 2012 (OVIDE/CATARINA cruise). This allowed the computing of CFC-based age with the Transit Time Distribution (TTD) method. Using the water mass distribution along GEOVIDE given by García-Ibáñez et al. (2018) and the distribution for the same water masses in 2012 (García-Ibáñez et al., 2015), we derived CFC-based ages for GEOVIDE waters (Fig. 6; further details in Supplemental Information S2). Uncertainties (1 standard error) associated with CFC-based age calculated with this approach range between 11-40%.

CFC-based water-mass ages range from ≈10 years, observed in DSOW at the bottom of the LA Sea, to ≈800 years, observed for NEADW at the bottom of the WE Basin. Because this study focuses on understanding controls on ^{231}Pa and ^{230}Th in recently ventilated waters, we omit detailed consideration of the upper 1km in subsequent discussion, and restrict our analysis to water sampled west of 35ºW of the section where young waters (<50 years) dominate. A rescaled version of the CFC age

section indicates the variation in age of ventilated waters (Fig. 6b). DSOW, occupying the deepest LA and IR Seas, is the youngest water mass in this region, with an average age of ~19 years. ISOW and LSW are slightly older, with ages ranging from 26 to 45 years and 32 to 40 years respectively.

4.2 Evolution of ^{230}Th and ^{231}Pa with water age

The presence of recently ventilated deep-waters with constrained CFC ages allows analysis of the rates at which ^{230}Th and ^{231}Pa concentrations increase during transport, and the rates of scavenging of these nuclides. To conduct this analysis, we define five components in the budget of ^{230}Th and ^{231}Pa:

i. Preformed component: The ^{230}Th or ^{231}Pa transported from the surface into the interior. For this analysis, in the absence of measurements for the exact location of deep-water formation during winter convection, we assume the same preformed value for all water masses and set this as the average of concentrations measured in surface waters <100 m depth along GEOVIDE section. This gives preformed concentrations of 1.66 µBq/kg for ^{230}Th and 1.31 µBq/kg for ^{231}Pa. We recognise that true preformed values may differ from these values and between water masses, and discuss the implications of uncertainty in preformed values in the following section. Preformed ^{230}Th and ^{231}Pa will decrease due to radioactive decay during transport. Although we take this decay into account in the following analysis, it is insignificant given the ages of waters involved and the much longer half-lives of ^{230}Th and ^{231}Pa.

ii. Ingrown component: The ingrown ^{230}Th or ^{231}Pa from radioactive decay of U since the water was last in contact with the surface. This component increases as the water mass ages. The concentration of this component in a water mass of age t can be calculated as:

$$^{230}Th_{Ingrown} = {}^{234}U \times (1 - e^{-\lambda_{230} t}) \qquad (4.1)$$

$$^{231}Pa_{Ingrown} = {}^{235}U \times (1 - e^{-\lambda_{231} t}) \qquad (4.2)$$

where $^{230}Th_{Ingrown}$ and $^{231}Pa_{Ingrown}$ are the ^{230}Th and ^{231}Pa ingrown from their U parents, respectively; ^{234}U and ^{235}U are activities of ^{234}U, and ^{235}U in seawater (45551.2 µBq/kg (2801.4 dpm/1000l) and 1823.8 µBq/kg (112.2 dpm/1000l), respectively, assuming a constant seawater ^{238}U activity of 39609.8 µBq/kg (2436 dpm/1000l) at salinity 35 psu, and seawater ^{234}U/^{238}U activity ratio of 1.15 and natural ^{238}/^{235}U abundance ratio of 137.88); λ_{230} and λ_{231} are decay constants of ^{230}Th and ^{231}Pa (9.17 $\times 10^{-6}$ yr^{-1} and 2.12×10^{-5} yr^{-1}, respectively).

iii. Potential Total component: The ^{230}Th and ^{231}Pa expected in the water due to the combination of preformed and ingrown components, if there were no removal by scavenging.

iv. Observed component: The ^{230}Th and ^{231}Pa observed in the water column, i.e. dissolved ^{230}Th and ^{231}Pa measured in this study (after correction for detritus and ingrowth from U since sample collection).

v. Scavenged component: The net ^{230}Th or ^{231}Pa removed from the water since it left the surface due to scavenging. For each depth, this component is the net of nuclide added from above by desorption from settling particles, and the removal downwards by scavenging.

These components are related to each other as follows:

$$Preformed + Ingrown = Potential\ Total\ ^{230}Th\ (or\ ^{231}Pa) = Observed + Scavenged \quad (4.3)$$

The difference between the Potential Total and the Observed concentration of ^{230}Th (or ^{231}Pa), therefore provides a measure of the amount of nuclide scavenged since the water left the surface (Fig. 7).

We examine the evolution of both the observed and scavenged components of ^{230}Th and ^{231}Pa with water mass age (Fig. 8). Both ^{230}Th and ^{231}Pa show an increase in observed concentration with age of water, with the increase for ^{230}Th much more regular than for ^{231}Pa. This strong ^{230}Th relationship, regardless of depth of the sample (Fig. 8a), indicates a primary control of water-mass age on the increase of ^{230}Th in these younger waters.

For ^{230}Th, the rate of increase with age (i.e. slope in Fig. 8a) indicates that about one quarter of the ^{230}Th formed from U decay remains in the water, with the other three quarters being removed by scavenging. This ratio is consistent with the average ^{230}Th for these waters, which requires that about three times more ^{230}Th than remains in water has been removed by scavenging (Fig. 8a, 8b). The scatter between ^{231}Pa and age (Fig. 8c) precludes the use of the slope to assess the relative proportion of scavenged ^{231}Pa, but the average values (Fig. 8c, 8d) indicate that about half of the ^{231}Pa remains in the water, while half is removed by scavenging. The relative behaviour of ^{230}Th and ^{231}Pa is consistent with previous expectations, with a higher fraction of scavenging of ^{230}Th than ^{231}Pa.

The hypothesis that ^{231}Pa/^{230}Th ratios increase monotonically as water mass ages forms the foundation of the Water-mass Evolution model for interpretation of sedimentary ^{231}Pa/^{230}Th in terms of the rate of deep water circulation. For these young waters, however, there is no clear relationship between observed ^{231}Pa/^{230}Th and age (Fig. 8e), nor between the ^{231}Pa/^{230}Th value scavenged to the sediment and age (Fig. 8f), calling the Water-mass Evolution model into question.

4.3 The importance of preformed ^{230}Th and ^{231}Pa in young waters

To assess the controls on ^{230}Th, ^{231}Pa, and particularly the resulting ^{231}Pa/^{230}Th ratio, we apply a simple scavenging-mixing model following Moran et al. (1997). This model was first created to assess the evolution of ^{230}Th in a 1D water column as it ages following ventilation. Here we adopt it by modelling the nuclide evolution with age for each depth, and by also modelling ^{231}Pa. This assumes that waters have remained at the same depth since ventilation which, though not correct in detail, still allows the model to provide insights about controls on these nuclides.

Following Moran et al. (1997), dissolved concentration of ^{230}Th and ^{231}Pa is given by,

$$c_d = \frac{C_{pre,t} + P \quad \tau_w}{(K_d\ SPM+1)} \times [1 - \exp(-\frac{(K_d\ SPM+1)}{SK_d\ \tau_w SPM} \times z)] \quad (4.4)$$

where C_d is the dissolved concentration of the nuclide ; P is the production rate of ^{230}Th and ^{231}Pa, 0.42 µBq/kg/yr (2.57 × 10^{-2} dpm/1000l/yr) and 0.039 µBq/kg/yr (2.37 × 10^{-3} dpm/1000l/yr), respectively; K_d is the distribution coefficient of the nuclide; λ is the decay constant of the nuclide; $C_{pre,t}$ is the preformed total concentration of ^{230}Th (or ^{231}Pa); SPM is the suspended particle concentration; and S is the particle settling speed, which represents the net effect of particle sinking, disaggregation and aggregation; τ_w is water mass age; z is the water depth.

Formatted: Normal, Left, Line spacing: single

Formatted: Font: (Asian) +Body Asian (SimSun), Font color: Auto

The model requires values for four parameters: particle settling speed (S), suspended particle concentration (SPM), and distribution coefficients for ^{230}Th (K_d^{Th}) and ^{231}Pa (K_d^{Pa}). We select these parameters to give a good fit to the ^{230}Th and ^{231}Pa observations at an open ocean station, Station 13, on the east of the section (i.e. a station sampling older waters, which are close to equilibrium) and use these values to interpret the younger waters to the west. Best fits to Station 13 suggested S = 800 m/yr; SPM = 25 µg/l; K_d^{Th} =1.1×10^7 ml/g; and K_d^{Pa} = 1.4×10^6 ml/g (the first three of these are close to those of Moran et al. (1997)). A fuller description of the model is given in Supplemental Information S3.

We show two sets of output from the model, one with a preformed component (C_{pre}) equal to the nuclide concentrations observed in the upper 100 m of the GEOVIDE section (as in 4.2 above), and one with the preformed component set to zero for both nuclides. For both cases, the modelled evolution of nuclide concentrations with age between 0-50 years at 2000 m and 3500 m water depths is plotted in Fig. 9, and compared to data. As expected, modeled ^{230}Th and ^{231}Pa concentrations increase with age, with deeper waters having higher concentrations and ^{230}Th increasing more rapidly initially (Fig. 9), but the preformed concentration is seen to be important in setting total nuclide concentration for several decades after ventilation. The fit of the model to observations in young waters from GEOVIDE is improved in the model run with zero preformed nuclide, particularly for ^{230}Th. This is surprising, given that surface-water ^{230}Th and ^{231}Pa values are generally non-zero, and typically close to the value observed in the GEOVIDE surface waters. For ^{230}Th in young deep waters, even the model with zero preformed nuclide overestimates the observed value, possibly indicating additional scavenging from these waters close to the seafloor, or as a result of differing biological productivity and particle fluxes between stations.

The most striking effect of changing the assumed preformed values in the model is on ^{231}Pa/^{230}Th (Fig. 9c). When preformed values are set at zero, ^{231}Pa/^{230}Th ratios always increase with water age, but when set at the average surface value from GEOVIDE, ^{231}Pa/^{230}Th ratios initially decrease before increasing. The impact of preformed concentrations has a long-lasting impact on water-column and scavenged ^{231}Pa/-Th, lasting for hundreds of years following ventilation (Supplementary Information Figure S2 (c), (d)). This indicates that knowledge of the nuclide concentration at the site of deep-water formation is critical to understanding the early evolution of ^{231}Pa/^{230}Th in waters and their underlying sediments.

4.4 Scavenging of ^{230}Th and ^{231}Pa

Knowledge of the CFC ages of the waters analysed on the GEOVIDE cruise allow an assessment of the scavenging rates of ^{230}Th and ^{231}Pa. To do so, we compare the Scavenged component to the Potential Total component (as defined in Section 4.2).

The percentage of the Scavenged component relative to the Potential Total component is higher for ^{230}Th, at an average of 80%, than for ^{231}Pa at an average of 40% (Fig. 10), consistent with the relatively higher particle-reactivity of ^{230}Th. For both nuclides, there is a higher fraction of scavenging in samples from near the seafloor, particularly those from DSOW in the deepest LA Sea. Bottom scavenging has been indicated in previous studies (e.g. Bacon and Anderson, 1982; Deng et al., 2014; Okubo et al., 2012), but this study indicates that this enhanced nuclide scavenging occurs even in the very young overflow waters at the start of the meridional circulation.

Deleted: An analysis of uncertainty of this assessment is given in Supplemental Information S4.

4.5 Uncertainty analysis of the assessment of the scavenging of ^{230}Th and ^{231}Pa

Uncertainty in both CFC-based ages and in preformed values of ^{230}Th and ^{231}Pa contribute to uncertainty when calculating the scavenging of ^{230}Th and ^{231}Pa. Uncertainties associated with CFC-based age range between 11-40% (1 standard error). This uncertainty leads to an average uncertainty of 23% and 13% in potential total ^{230}Th and ^{231}Pa respectively, corresponding to an average uncertainty of 30% in the scavenged component of ^{230}Th and 40% in the scavenged component of ^{231}Pa.

A two-fold increase in preformed values results in an increase by a factor of 1.2 and 1.6 in the total potential ^{230}Th and ^{231}Pa, respectively, leading to an increase by a factor of 1.2 in the scavenged component of ^{230}Th and of 2.6 in the scavenged component of ^{231}Pa. The impact of preformed uncertainty is less significant when comparing the scavenging to the potential total components. The ratio of scavenged/potential total increases by a factor of 1.1 and 1.4 for ^{230}Th and ^{231}Pa, respectively. This sensitivity analysis indicates that a better knowledge of preformed values will benefit the assessment of the scavenging of both nuclides.

Formatted: Normal, Left, Line spacing: single

Formatted: Font color: Auto, English (US)

4.6 Meridional transport of ^{230}Th and ^{231}Pa in the North Atlantic

Deleted: 5

Previous calculations have indicated removal of ^{230}Th and ^{231}Pa from the North Atlantic by meridional transport southward. Deng et al. (2014) calculated net southward transport of 6% of the ^{230}Th and 33% of ^{231}Pa, relative to production of these nuclides in the water column. That calculation, however, did not provide a complete budget for ^{230}Th and ^{231}Pa for the North Atlantic because observations at the time did not constrain input of these nuclides from the north. Data in this study allow this calculation, and therefore a more complete budget for the modern North Atlantic.

García-Ibáñez et al. (2018) calculated volume transports for the Portugal to Greenland section of the GEOVIDE section by combining the water mass fractions from eOMP analysis with the absolute geostrophic velocity field calculated using inverse model constrained by Doppler current profiler velocity measurements (Zunino et al., 2017). They separated northward flowing upper, and southward flowing lower limbs of the AMOC at isopycnal σ_1 (potential density referenced to 1000 dbar) = 32.15 kg/m^3, with +18.7 ± 2.4 Sv and -17.6 ± 3.0 Sv flow across the section above and below this value (positive value indicates northward transport). With average ^{230}Th and ^{231}Pa concentrations in the upper limb (σ_1 < 32.15 kg/m^3) of 1.60 and 1.32 µBq/kg respectively, northward transport of ^{230}Th is 3.07×10^{10} and of ^{231}Pa is 2.53×10^{10} µBq/s. Average ^{230}Th and ^{231}Pa

concentrations in the lower limb ($\sigma_1 > 32.15$ kg/m^3) are 3.44 and 2.07 μBq/kg , respectively, indicating transports of ^{230}Th and ^{231}Pa are -6.22 × 10^{10} and -3.74 × 10^{10} μBq/s, respectively.

Net transport of ^{230}Th and ^{231}Pa across GEOVIDE is therefore to the south, and supplies 3.15 × 10^{10} μBq/s ^{230}Th and 1.21 × 10^{10} μBq/s ^{231}Pa to the North Atlantic (Fig. 11). This is a smaller net transport than further south in the Atlantic (Fig. 11), due to the lower ^{230}Th and ^{231}Pa concentrations in the water column close of the site of deep-water formation.

The budget for these nuclides for the North Atlantic consists of: production in the water column; addition by advection from the North; loss by advection to the South and removal to the sediment. The data from this study allows this budget to be fully assessed, and indicates that the flux to the sediment is equivalent to 96% of the production of ^{230}Th, and 74% of the production for ^{231}Pa (Supplemental Information Table S4). For both nuclides, these fluxes are higher than in previous calculations (Deng et al., 2014) which ignored advective fluxes from the North. There is, however, still a significantly higher advective loss of ^{231}Pa relative to ^{230}Th. At a basin scale, therefore, ^{231}Pa/^{230}Th in the sediment must be lower than the production ratio. This lower value is generated by the meridional transport of the North Atlantic, and likely to be sensitive to changes in this transport. Use the Basin-scale Advection model to interpret sedimentary ^{231}Pa/^{230}Th to assess meridional transport, as initially proposed by Yu et al. (1996), is therefore still supported by a full modern North Atlantic budget for these nuclides.

Deleted: 5

5 Conclusion

Measurement of ^{230}Th and ^{231}Pa in waters from GEOVIDE show some control of water mass on ^{230}Th and ^{231}Pa concentrations, particularly low concentrations in DSOW and high values in the old NEADW. There is, however, no close mapping of nuclide concentration to water mass.

With the availability of CFC-based ages on this section, the evolution of ^{230}Th and ^{231}Pa concentration with age is possible. A systematic increase of ^{230}Th concentration is observed over the first 50 years following ventilation, and a similar though more scattered relationship seen for ^{231}Pa. There is no clear relationship between the ^{231}Pa/^{230}Th ratio and age for these young waters The long-term evolution of ^{231}Pa/^{230}Th is found from a simple model to be highly dependent on the preformed concentrations for these nuclides. These results complicate the interpretation of sedimentary ^{231}Pa/^{230}Th as a paleo-proxy for deep water circulation based on systematic evolution of water ^{231}Pa/^{230}Th with age, and point to the importance of a better knowledge of preformed ^{230}Th and ^{231}Pa concentrations to improve interpretation. This analysis of the ^{230}Th and ^{231}Pa concentration relative to the age of the water not only demonstrates the influence of water mass aging on ^{231}Pa and ^{230}Th, but also points to the influence of scavenging. Scavenged ^{230}Th is much more extensive than ^{231}Pa, as expected, and enhanced removal of both nuclides is seen immediately above the seafloor, particularly for young waters.

Calculation of meridional transport of ^{230}Th and ^{231}Pa indicates a southward net transport of both nuclides across the GEOVIDE section. This advection is smaller than that further south in the Atlantic as a result of lower ^{230}Th and ^{231}Pa concentrations at GEOVIDE. Calculation of the flux across GEOVIDE allows a more complete budget for the North Atlantic to be constructed and demonstrates a significantly higher advective loss of ^{231}Pa to the south relative to ^{230}Th, with 26% of the

^{231}Pa produced advected southward (relative to only 4% for ^{230}Th). This calculation supports the interpretation of sedimentary ^{231}Pa/^{230}Th measurements as a proxy for overturning circulation, when based on advective loss of ^{231}Pa at a basin scale.

Acknowledgements

Géraldine Sarthou and Pascale Lherminier are thanked for leading the GEOVIDE cruise, along with the captain, Gilles Ferrand, and crew of the R/V Pourquoi Pas?. We would like to give a special thanks to Pierre Branellec, Floriane Desprez de Gésincourt, Michel Hamon, Catherine Kermabon, Philippe Le Bot, Stéphane Leizour, Olivier Ménage, Fabien Pérault and Emmanuel de Saint Léger for their technical expertise and to Catherine Schmechtig for the GEOVIDE database management. This work was supported by the French National Research Agency (ANR-13-BS06-0014, ANR-12-PDOC-0025-01), the French National Centre for Scientific Research (CNRS-LEFE-CYBER), the LabexMER (ANR-10-LABX-19), and Ifremer. It was supported for the logistic by DT-INSU and GENAVIR. Thank you also to Yi Tang who helped with sampling during the cruise. We are grateful to Mercedes de la Paz Arandiga, and Pascale Lherminier for providing valuable input during analysis of water masses and ages, and to Maribel García-Ibáñez for early provision of the eOMP analysis presented elsewhere in this volume. We also thank Yves Plancherel for valuable insight during discussion of the results presented.

References

Anderson, R. F., Bacon, M. P. and Brewer, P. G.: Removal of ^{230}Th and ^{231}Pa at ocean margins, Earth Planet. Sci. Lett., 66, 73–90, doi:https://doi.org/10.1016/0012-821X(83)90127-9, 1983a.

Anderson, R. F., Bacon, M. P. and Brewer, P. G.: Removal of ^{230}Th and ^{231}Pa from the open ocean, Earth Planet. Sci. Lett., 62(1), 7–23, doi:https://doi.org/10.1016/0012-821X(83)90067-5, 1983b.

Anderson, R. F., Fleisher, M. Q., Biscaye, P. E., Kumar, N., Dittrich, B., Kubik, P. and Suter, M.: Anomalous boundary scavenging in the Middle Atlantic Bight: evidence from ^{230}Th, ^{231}Pa, ^{10}Be and ^{210}Pb, Deep Sea Res. Part II Top. Stud. Oceanogr., 41(2), 537–561, doi:https://doi.org/10.1016/0967-0645(94)90034-5, 1994.

Anderson, R. F., Fleisher, M. Q., Robinson, L. F., Edwards, R. L., Hoff, J. A., Moran, S. B., Rutgers van der Loeff, M. R., Thomas, A. L., Roy-Barman, M. and Francois, R.: GEOTRACES intercalibration of ^{230}Th, ^{232}Th, ^{231}Pa, and prospects: For ^{10}Be, Limnol. Oceanogr. Methods, 10(APRIL), 179–213, doi:10.4319/lom.2012.10.179, 2012.

Bacon, M. P. and Anderson, R. F.: Distribution of thorium isotopes between dissolved and particulate forms in the deep sea, J. Geophys. Res., 87(C3), 2045, doi:10.1029/JC087iC03p02045, 1982.

Bradtmiller, L. I., McManus, J. F. and Robinson, L. F.: ^{231}Pa/^{230}Th evidence for a weakened but persistent Atlantic meridional overturning circulation during Heinrich Stadial 1, Nat. Commun., 5, 5817 [online] Available from: http://dx.doi.org/10.1038/ncomms6817, 2014.

Chase, Z., Anderson, R. F., Fleisher, M. Q. and Kubik, P. W.: The influence of particle composition and particle flux on

scavenging of Th, Pa and Be in the ocean, Earth Planet. Sci. Lett., 204(1), 215–229, doi:https://doi.org/10.1016/S0012-821X(02)00984-6, 2002.

Cheng, H., Edwards, L.R., Shen, C.-C., Polyak, V. J., Asmerom, Y., Woodhead, J., Hellstrom, J., Wang, Y., Kong, X., Spötl, C., Wang, X. and Calvin, A. E.: Improvements in ^{230}Th dating, ^{230}Th and ^{234}U half-life values, and U–Th isotopic measurements by multi-collector inductively coupled plasma mass spectrometry, Earth Planet. Sci. Lett., 371, 82–91, doi:10.1016/j.epsl.2013.04.006, 2013.

Deng, F., Thomas, A. L., Rijkenberg, M. J. A. and Henderson, G. M.: Controls on seawater ^{231}Pa, ^{230}Th and ^{232}Th concentrations along the flow paths of deep waters in the Southwest Atlantic, Earth Planet. Sci. Lett., 390, 93–102, doi:https://doi.org/10.1016/j.epsl.2013.12.038, 2014.

Dickson, R. R. and Brown, J.: The production of North Atlantic Deep Water: Sources, rates, and pathways, J. Geophys. Res. Ocean., 99(C6), 12319–12341, doi:10.1029/94JC00530, 1994.

Falina, A., Sarafanov, A., Mercier, H., Lherminier, P., Sokov, A. and Daniault, N.: On the Cascading of Dense Shelf Waters in the Irminger Sea, J. Phys. Oceanogr., 42(12), 2254–2267, doi:10.1175/JPO-D-12-012.1, 2012.

García-Ibáñez, M. I., Pardo, P. C., Carracedo, L. I., Mercier, H., Lherminier, P., Ríos, A. F. and Pérez, F. F.: Structure, transports and transformations of the water masses in the Atlantic Subpolar Gyre, Prog. Oceanogr., 135, 18–36, doi:https://doi.org/10.1016/j.pocean.2015.03.009, 2015.

García-Ibáñez, M. I., Pérez, F. F., Lherminier, P., Zunino, P., Mercier, H. and Tréguer, P.: Water mass distributions and transports for the 2014 GEOVIDE cruise in the North Atlantic, Biogeosciences, 15(7), 2057–2090 [online] Available from: https://doi.org/10.5194/bg-15-2075-2018, 2018.

Gherardi, J.-M., Labeyrie, L., McManus, J. F., Francois, R., Skinner, L. C. and Cortijo, E.: Evidence from the Northeastern Atlantic basin for variability in the rate of the meridional overturning circulation through the last deglaciation, Earth Planet. Sci. Lett., 240(3), 710–723, doi:https://doi.org/10.1016/j.epsl.2005.09.061, 2005.

Gherardi, J. M., Labeyrie, L., Nave, S., Francois, R., McManus, J. F. and Cortijo, E.: Glacial-interglacial circulation changes inferred from ^{231}Pa/^{230}Th sedimentary record in the North Atlantic region, Paleoceanography, 24(2), doi:doi:10.1029/2008PA001696, 2009.

Hayes, C. T., Anderson, R. F., Fleisher, M. Q., Serno, S., Winckler, G. and Gersonde, R.: Biogeography in ^{231}Pa/ ^{230}Th ratios and a balanced ^{231}Pa budget for the Pacific Ocean, Earth Planet. Sci. Lett., 391, 307–318, doi:10.1016/j.epsl.2014.02.001, 2014.

Hayes, C. T., Anderson, R. F., Fleisher, M. Q., Huang, K. F., Robinson, L. F., Lu, Y., Cheng, H., Edwards, R. L. and Moran, S. B.: ^{230}Th and ^{231}Pa on GEOTRACES GA03, the U.S. GEOTRACES North Atlantic transect, and implications for modern and paleoceanographic chemical fluxes, Deep. Res. Part II Top. Stud. Oceanogr., 116, 29–41, doi:10.1016/j.dsr2.2014.07.007, 2015.

Henderson, G. M. and Anderson, R. F.: The U-series Toolbox for Paleoceanography, Rev. Mineral. Geochemistry, 52(1), 493–531 [online] Available from: http://dx.doi.org/10.2113/0520493, 2003.

Holden, N. E.: Total half-lives for selected nuclides, Pure Appl. Chem., 62, 941, doi:10.1351/pac199062050941, 1990.

de la Paz, M., García-Ibáñez, M. I., Steinfeldt, R., Ríos, A. F. and Pérez, F. F.: Ventilation versus biology: What is the controlling mechanism of nitrous oxide distribution in the North Atlantic?, Global Biogeochem. Cycles, 31(4), 745–760, doi:10.1002/2016GB005507, 2017.

Luo, Y., Francois, R. and Allen, S. E.: Sediment $^{231}Pa/^{230}Th$ as a recorder of the rate of the Atlantic meridional overturning circulation: insights from a 2-D model, Ocean Sci., 6(1), 381–400, doi:10.5194/os-6-381-2010, 2010.

Marchal, O., François, R., Stocker, T. F. and Joos, F.: Ocean thermohaline circulation and sedimentary $^{231}Pa/^{230}Th$ ratio, Paleoceanography, 15(6), 625–641, doi:10.1029/2000PA000496, 2010.

McManus, J. F., Francois, R., Gherardi, J.-M., Keigwin, L. D. and Brown-Leger, S.: Collapse and rapid resumption of Atlantic meridional circulation linked to deglacial climate changes, Nature, 428, 834 [online] Available from: http://dx.doi.org/10.1038/nature02494, 2004.

Moran, S. B., Charette, M. A., Hoff, J. A. and Edwards, R. L.: Distribution of 230Th in the Labrador Sea and its relation to ventilation, Earth Planet. Sci. Lett., 150, 151–160, 1997.

Moran, S. B., Shen, C., Edmonds, H. N., Weinstein, S. E., Smith, J. N. and Edwards, R. L.: Dissolved and particulate ^{231}Pa and ^{230}Th in the Atlantic Ocean : constraints on intermediate / deep water age , boundary scavenging , and $^{231}Pa/^{230}Th$ fractionation, Earth Planet. Sci. Lett., 203, 999–1014, 2002.

Negre, C., Zahn, R., Thomas, A. L., Masqué, P., Henderson, G. M., Martínez-Méndez, G., Hall, I. R. and Mas, J. L.: Reversed flow of Atlantic deep water during the Last Glacial Maximum, Nature, 468, 84 [online] Available from: http://dx.doi.org/10.1038/nature09508, 2010.

Nozaki, Y., Horibe, Y. and Tsubota, H.: The water column distributions of thorium isotopes in the western North Pacific, Earth Planet. Sci. Lett., 54(2), 203–216, doi:https://doi.org/10.1016/0012-821X(81)90004-2, 1981.

Okubo, A., Obata, H., Gamo, T. and Yamada, M.: ^{230}Th and ^{232}Th distributions in mid-latitudes of the North Pacific Ocean: Effect of bottom scavenging, Earth Planet. Sci. Lett., 339–340, 139–150, doi:10.1016/j.epsl.2012.05.012, 2012.

Olsson, K. A., Jeansson, E., Anderson, L. G., Hansen, B., Eldevik, T., Kristiansen, R., Messias, M.-J., Johannessen, T. and Watson, A. J.: Intermediate water from the Greenland Sea in the Faroe Bank Channel: spreading of released sulphur hexafluoride, Deep Sea Res. Part I Oceanogr. Res. Pap., 52(2), 279–294, doi:https://doi.org/10.1016/j.dsr.2004.09.009, 2005.

Regelous, M., Turner, S., Elliott, T., Rostami, K. and Hawkesworth, C.: Measurement of Femtogram Quantities of Protactinium in Silicate Rock Samples by Multicollector Inductively Coupled Plasma Mass Spectrometry, Anal. Chem., 76(1), doi:10.1021/ac702316r, 2004.

Rempfer, J., Stocker, T. F., Joos, F., Lippold, J. and Jaccard, S. L.: New insights into cycling of ^{231}Pa and ^{230}Th in the Atlantic Ocean, Earth Planet. Sci. Lett., 468, 27–37, doi:https://doi.org/10.1016/j.epsl.2017.03.027, 2017.

Robert, J., Miranda, C. F. and Muxart, R.: Mesure de la période du protactinium 231 par microcalorimétrie, Radiochim. Acta, 11(2), 104–108, doi:10.1524/ract.1969.11.2.104, 1969.

Roberts, N. L., McManus, J. F., Piotrowski, A. M. and McCave, I. N.: Advection and scavenging controls of Pa/Th in the

northern NE Atlantic, Paleoceanography, 29(6), 668–679, doi:10.1002/2014PA002633, 2014.

Robinson, L. F., Belshaw, N. S. and Henderson, G. M.: U and Th concentrations and isotope ratios in modern carbonates and waters from the Bahamas, Geochim. Cosmochim. Acta, 68(8), 1777–1789, doi:https://doi.org/10.1016/j.gca.2003.10.005, 2004.

Rutgers van der Loeff, M. M. and Berger, G. W.: Scavenging of ^{230}Th and ^{231}Pa near the antarctic polar front in the South Atlantic, Deep Sea Res. Part I Oceanogr. Res. Pap., 40(2), 339–357, doi:https://doi.org/10.1016/0967-0637(93)90007-P, 1993.

Saunders, P, M.: Chapter 5.6 The dense northern overflows, in Ocean Circulation and Climate, vol. 77, edited by G. Siedler, J. Church, and J. B. T.-I. G. Gould, pp. 401–417, Academic Press., 2001.

Siddall, M., Henderson, G. M., Edwards, N. R., Frank, M., Müller, S. A., Stocker, T. F. and Joos, F.: ^{231}Pa/^{230}Th fractionation by ocean transport, biogenic particle flux and particle type, Earth Planet. Sci. Lett., 237(1–2), 135–155, doi:10.1016/j.epsl.2005.05.031, 2005.

Siddall, M., Stocker, T. F., Henderson, G. M., Joos, F., Frank, M., Edwards, N. R., Ritz, S. P. and Müller, S. A.: Modeling the relationship between ^{231}Pa/^{230}Th distribution in North Atlantic sediment and Atlantic meridional overturning circulation, Paleoceanography, 22(2), doi:10.1029/2006PA001358, 2007.

Talley, L. D. and McCartney, M. S.: Distribution and Circulation of Labrador Sea Water, J. Phys. Oceanogr., 12(11), 1189–1205, doi:10.1175/1520-0485(1982)012<1189:DACOLS>2.0.CO;2, 1982.

Tanhua, T., Olsson, K. A. and Jeansson, E.: Formation of Denmark Strait overflow water and its hydro-chemical composition, J. Mar. Syst., 57(3), 264–288, doi:https://doi.org/10.1016/j.jmarsys.2005.05.003, 2005.

Thomas, A. L., Henderson, G. M. and Robinson, L. F.: Interpretation of the ^{231}Pa/ ^{230}Th paleocirculation proxy: New water-column measurements from the southwest Indian Ocean, Earth Planet. Sci. Lett., 241(3), 493–504, doi:https://doi.org/10.1016/j.epsl.2005.11.031, 2006.

Thomas, A. L., Henderson, G. M. and McCave, I. N.: Constant bottom water flow into the Indian Ocean for the past 140 ka indicated by sediment ^{231}Pa/^{230}Th ratios, Paleoceanography, 22(4), doi:10.1029/2007PA001415, 2007.

Usman, K. and MacMahon, T. D.: Determination of the half-life of ^{233}Pa, Appl. Radiat. Isot., 52(3), 585–589, doi:https://doi.org/10.1016/S0969-8043(99)00214-6, 2000.

Yashayaev, I. and Dickson, B.: Transformation and Fate of Overflows in the Northern North Atlantic BT - Arctic–Subarctic Ocean Fluxes: Defining the Role of the Northern Seas in Climate, edited by R. R. Dickson, J. Meincke, and P. Rhines, pp. 505–526, Springer Netherlands, Dordrecht., 2008.

Yu, E.-F., Francois, R. and Bacon, M. P.: Similar rates of modern and last-glacial ocean thermohaline circulation inferred from radiochemical data, Nature, 379, 689 [online] Available from: http://dx.doi.org/10.1038/379689a0, 1996.

Zunino, P., Lherminier, P., Mercier, H., Daniault, N., García-Ibáñez, M. I. and Pérez, F. F.: The GEOVIDE cruise in May–June 2014 reveals an intense Meridional Overturning Circulation over a cold and fresh subpolar North Atlantic, Biogeosciences, 14(23), 5323–5342, doi:10.5194/bg-14-5323-2017, 2017.

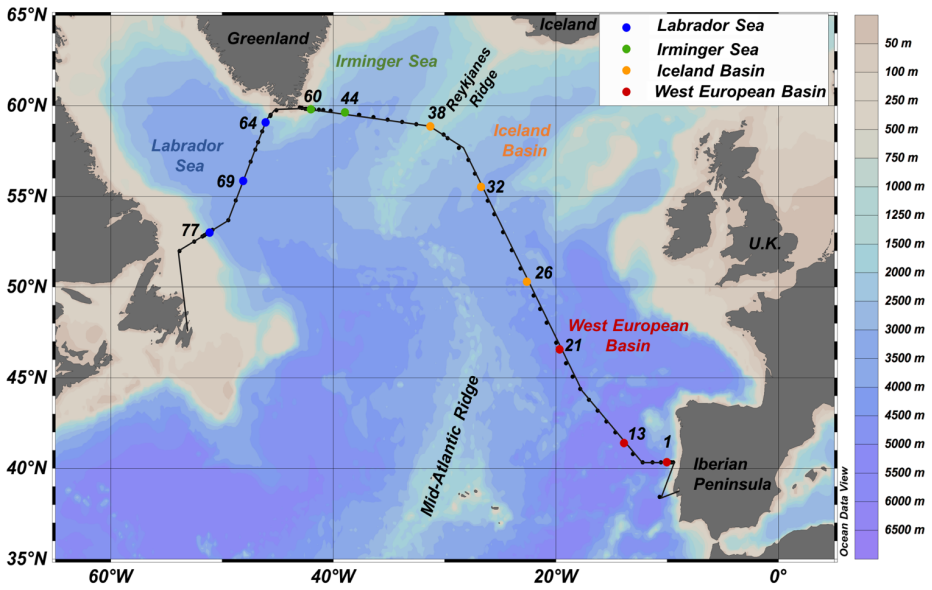

Figure 1: Map showing GEOVIDE cruise track (black line) and station locations (black dots). Colour bars indicate water depth. Sampling locations for water-column ^{231}Pa and ^{230}Th in this study are shown by coloured dots, with colours representing the ocean regions they are located in.

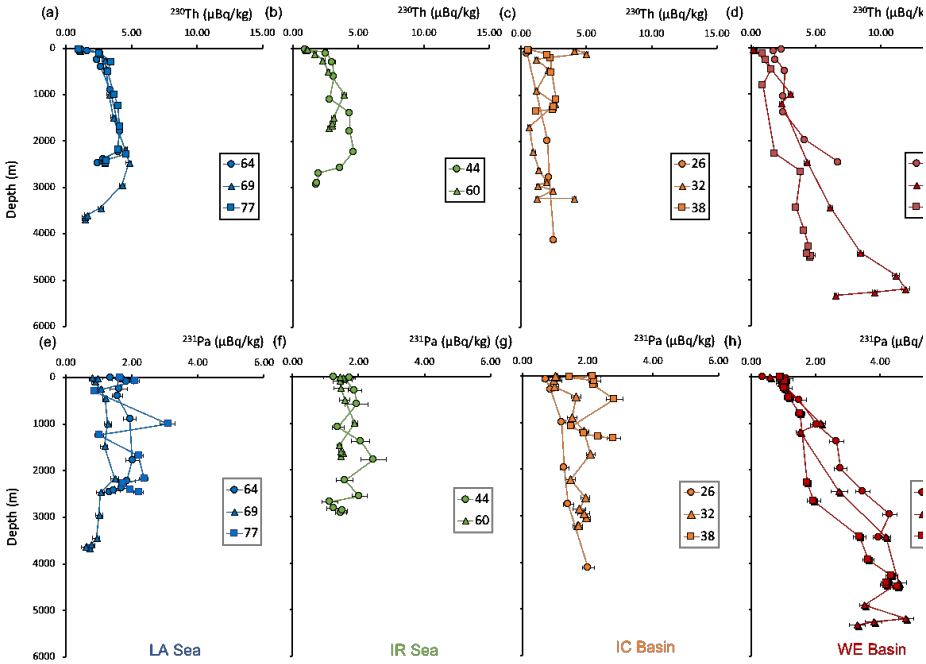

Figure 2: Vertical profiles of ^{230}Th (a-d) and ^{231}Pa (e-h) in the water column along the GEOVIDE section. Colours corresponds to the region (as in Fig. 1). LA = Labrador, IR = Irminger, IC = Iceland, WE = West European). Uncertainties represent 2 standard error (2 s.e.).

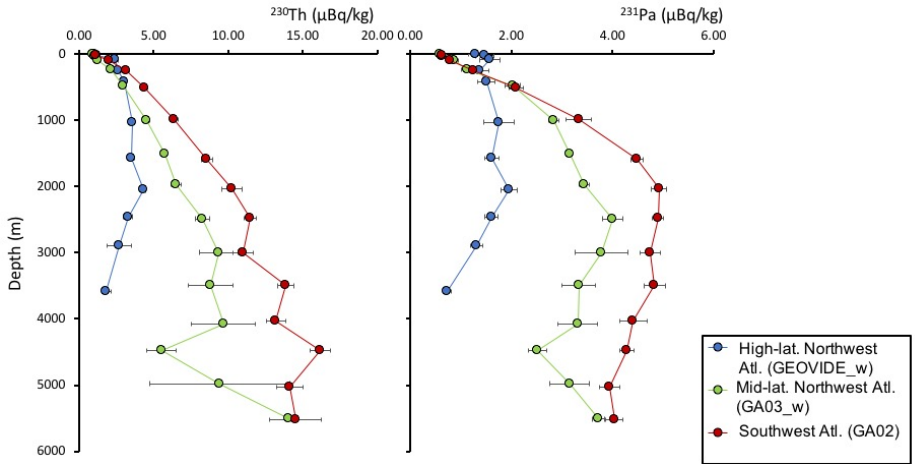

Figure 3: Vertical profiles of ^{230}Th and ^{231}Pa from high-latitude Northwest Atlantic (west section of GEOVIDE), mid-latitude Northwest Atlantic (GA03_w), and Southwest Atlantic (GA02). Data from all stations were sorted by water depth and averages for depth and ^{230}Th and ^{231}Pa concentrations were taken for surface, 25 m,100 m, 250 m, 500 m, and every 500 m interval below. Error bars on ^{230}Th and ^{231}Pa concentrations averages reflect standard deviation of the mean of measurements.

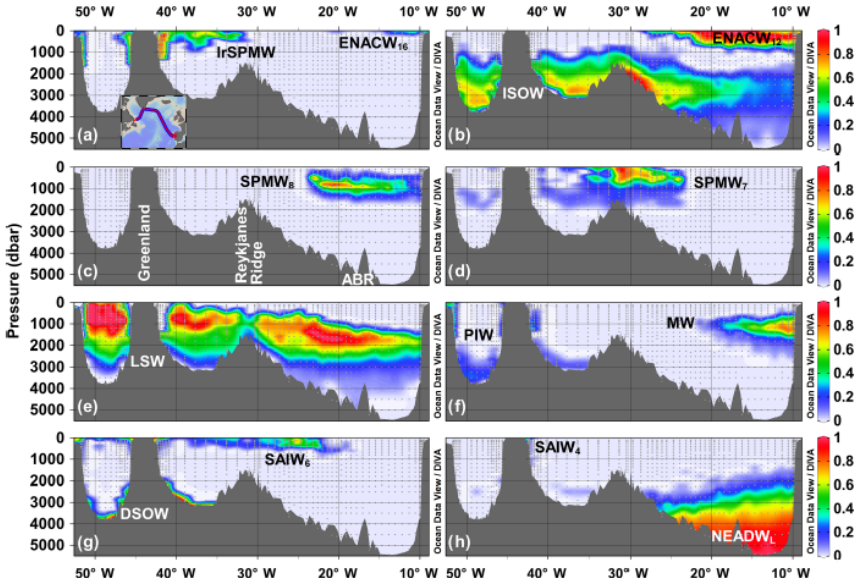

Figure 4: Results of Extended Optimum MultiParameter (eOMP) analysis for the GEOVIDE section (García-Ibáñez et al., 2018). Colours reflect the fraction of water at each location assigned to the water mass shown in that panel: $ENACW_{16}$ and $ENACW_{12}$ = East North Atlantic Central Water of 16ºC and 12ºC; $SPMW_8$, $SPMW_7$, IrSPMW = Subpolar Mode Water of 8ºC, 7ºC and of the Irminger Sea; $SAIW_6$ and $SAIW_4$ = Subarctic Intermediate Water of 6ºC and 4ºC; MW = Mediterranean Water; PIW = Polar Intermediate Water; ISOW=Iceland–Scotland Overflow Water; LSW=Labrador Sea Water; DSOW: Denmark Strait Overflow Waters; and $NEADW_L$: Lower North East Atlantic Deep Water; ABR= Azores-Biscay Rise.

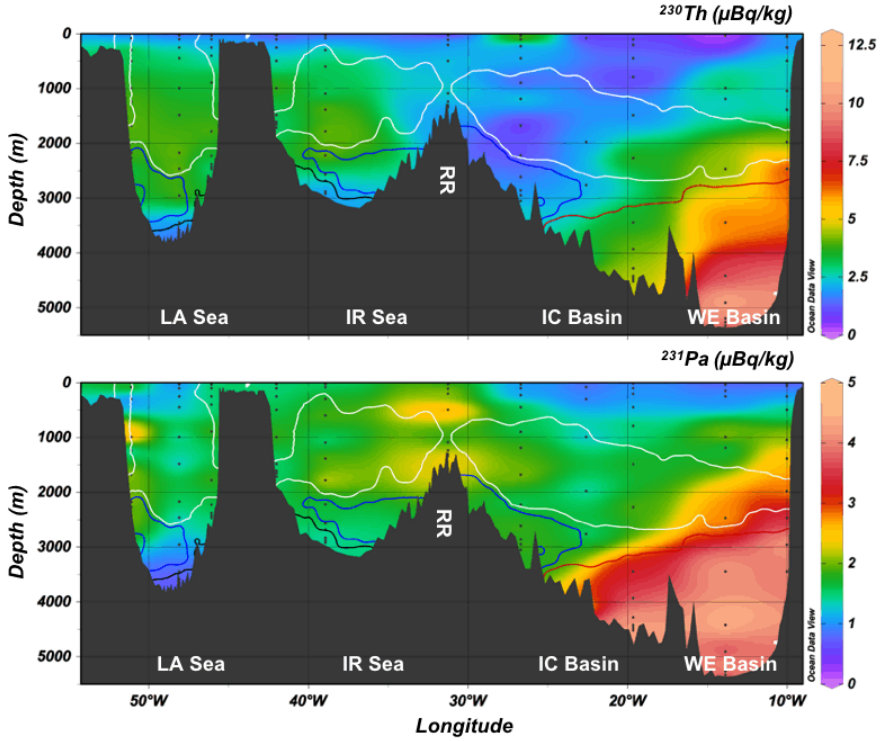

Figure 5: Distribution of ^{230}Th and ^{231}Pa along the GEOVIDE section. Water masses were indicated by contours (black: DSOW; blue: ISOW; white: LSW; red: NEADW.) based on 50% level percentage composition of source water types from eOMP analysis.

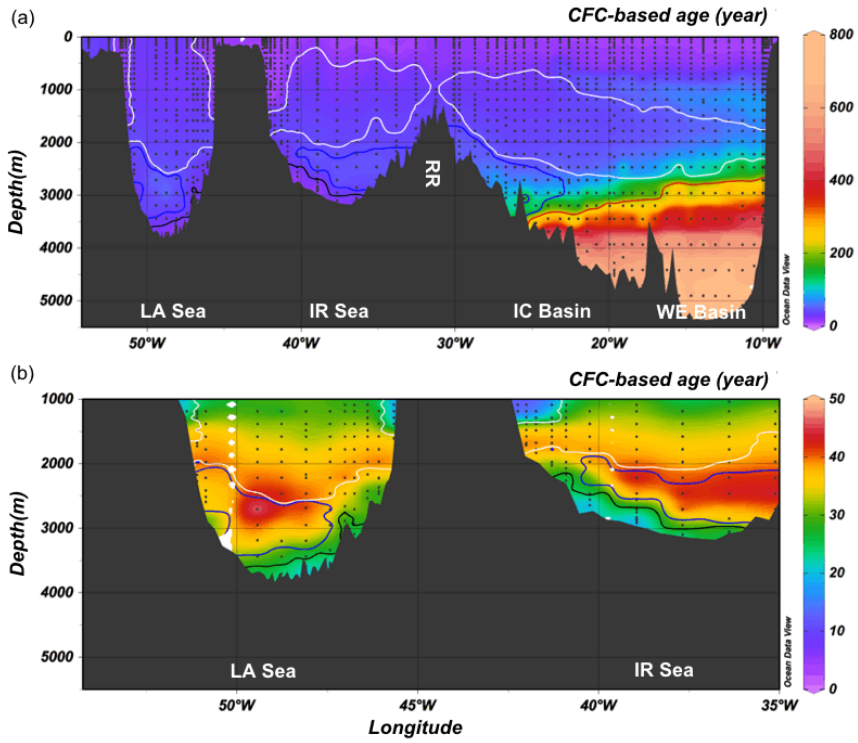

Figure 6: Water mass age based on CFC data along the GEOVIDE section. (a) Full water-column data for the entire section, showing waters from 10 to 800 years in age; (b) A rescaled version of (a) omitting the upper 1000m and the older waters east of 35°W to show age variation in recently ventilated deep-waters. Water masses were indicated by contours (black: DSOW; blue: ISOW; white: LSW; red: NEADW.) based on 50% level percentage composition of source water types from eOMP analysis.

Deleted:

Deleted: west

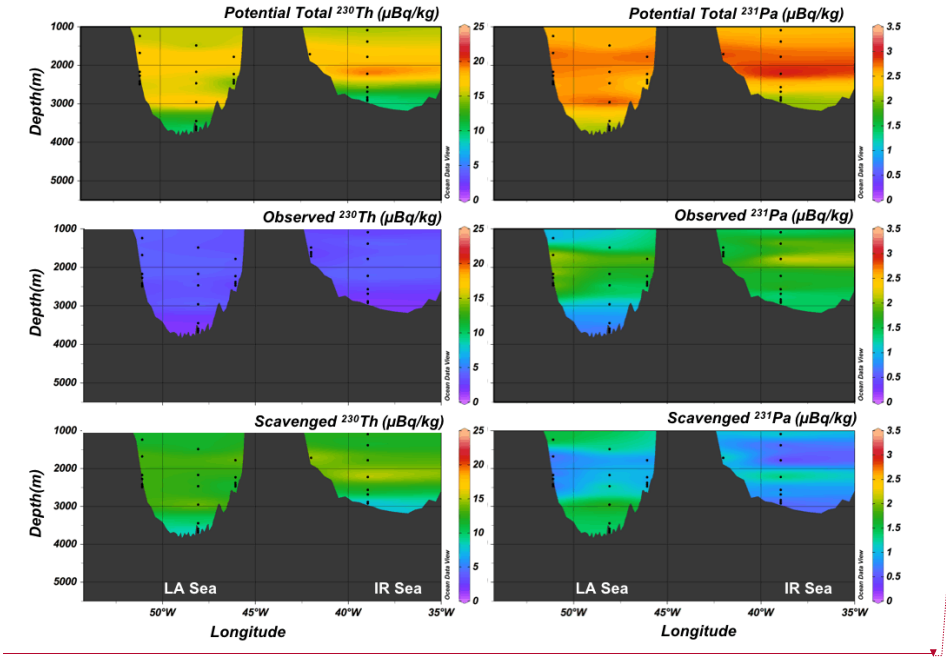

Deleted:

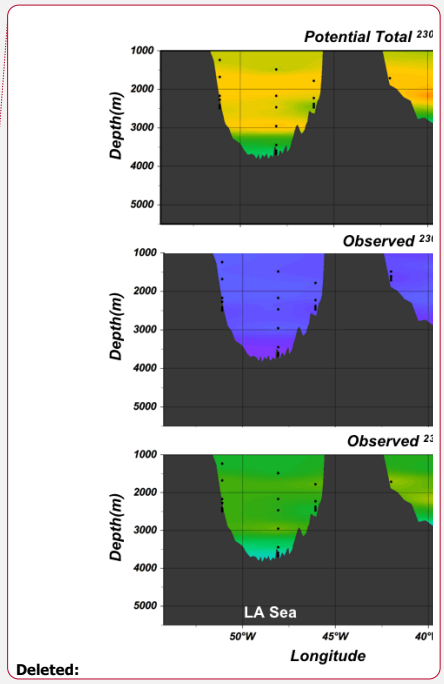

Figure 7: Potential Total, Observed, and Scavenged components of ^{230}Th and ^{231}Pa in waters >1000 m water depth and west of 35°W.

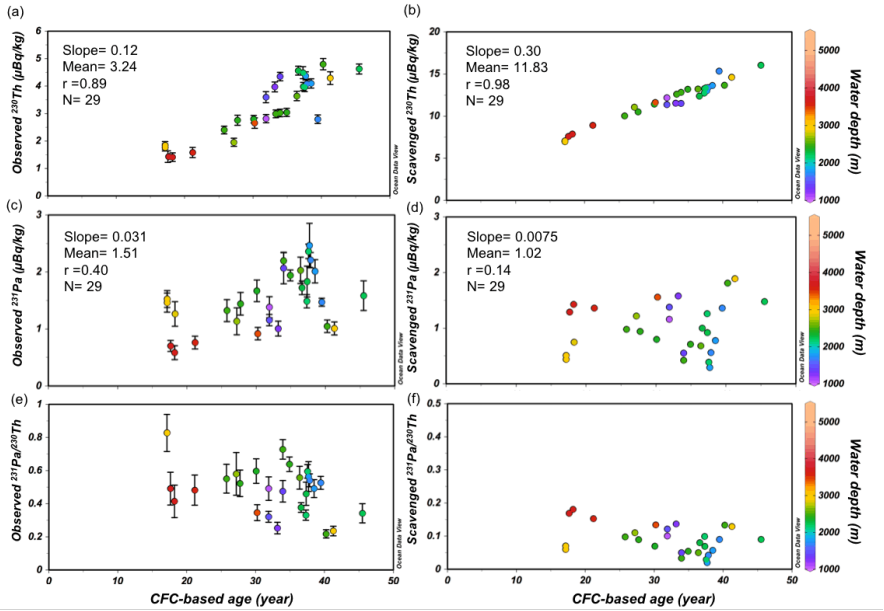

Figure 8: Relationship between water mass age and the Observed and Scavenged components of ^{230}Th, ^{231}Pa and ^{231}Pa/^{230}Th (colour coded by water depth). Least square fitting statistics were also given, i.e. slope and correlation coefficient r of the least square line, mean value and number of the data points. Note the increase of observed concentrations for both nuclides with age. Comparison of average values indicates that about three quarters of ^{230}Th produced by decay is scavenged, compared with about half of the ^{231}Pa.

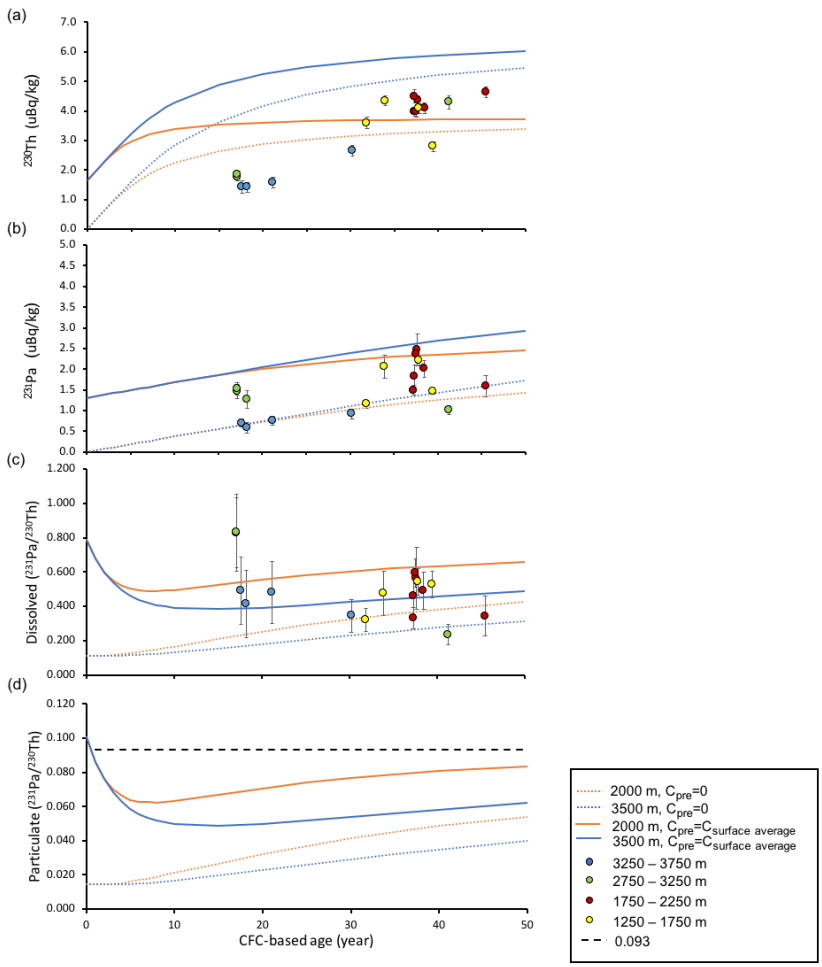

Figure 9: Results from a scavenging-mixing model of ^{230}Th, ^{231}Pa, Dissolved ^{231}Pa/^{230}Th and particulate ^{231}Pa/^{230}Th compared to observations. Preformed concentration (C_{pre}) were set at 0 (dashed line) and at the average surface concentration ($C_{surface\ average}$) from GEOVIDE section (solid line), i.e. ^{230}Th= 1.66 µBq/kg, ^{231}Pa= 1.31 µBq/kg. A version of this figure extending to older waters is available in the Supplemental Information Figure S2.

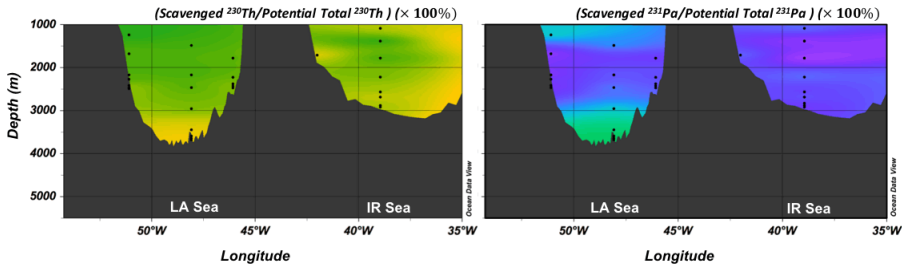

Figure 10: Ratio of Scavenged component to Potential Total component for ^{230}Th and ^{231}Pa, providing an assessment of the relative importance of scavenging for the two nuclides, and of the location of scavenging.

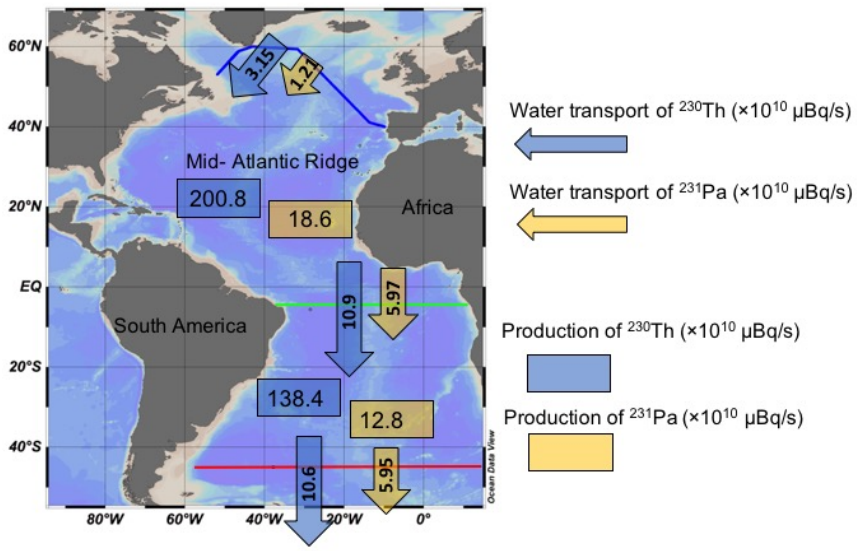

Figure 11: Fluxes of ^{230}Th (blue arrow) and ^{231}Pa (yellow arrow) across the GEOVIDE section (blue solid line), 4.5ºS (green solid line) and 45ºS (red solid line). Also shown are production of ^{230}Th (blue box) and ^{231}Pa (yellow box) in the North Atlantic (between GEOVIDE section and 4.5ºS) and in the South Atlantic (between 4.5ºS and 45ºS), based on calculation in Deng et al. (2014). These fluxes indicate that 4% of the ^{230}Th produced in the North Atlantic is exported southward by ocean circulation, and 26% of the ^{231}Pa.

Supplemental Information of

Evolution of ^{231}Pa and ^{230}Th in overflow waters of the North Atlantic

Feifei Deng et al.

Correspondence to: Feifei Deng (feifei.deng@earth.ox.ac.uk)

S1. Data of water-column ^{231}Pa, ^{230}Th and ^{232}Th concentrations, and $^{231}Pa/^{230}Th$ ratios along GEOVIDE section and details of correction

Table S1 Water-column ^{231}Pa, ^{230}Th and ^{232}Th concentrations, and $^{231}Pa/^{230}Th$ ratios along GEOVIDE section

Station	Depth	^{231}Pa	$^{231}Pa_{corr}$	$^{231}Pa_{corr}$	2se	^{230}Th	^{230}Th	$^{230}Th_{corr}$	2se	^{232}Th	^{232}Th	2se	$^{231}Pa/^{230}Th$	2se
	m	fg/kg	fg/kg	µBq/kg		fg/kg	fg/kg	µBq/kg		pg/kg	pmol/kg			
1	3445.3	2.270	2.269	3.96	0.17									
40.33°N	2955.3	2.465	2.463	4.30	0.22									
10.04°W	2465.8	1.988	1.982	3.46	0.22	9.00	8.83	6.72	0.20	52.33	0.2248	0.0046	0.516	0.036
	1974.9	1.592	1.588	2.77	0.19	5.64	5.50	4.18	0.17	43.47	0.1867	0.0036	0.663	0.053
	1385.3	1.522	1.517	2.65	0.23	3.43	3.28	2.50	0.14	44.96	0.1931	0.0041	1.061	0.108
	1039.6	1.176	1.170	2.04	0.20	3.48	3.29	2.50	0.20	59.80	0.2568	0.0049	0.818	0.105
	495.6	0.861	0.853	1.49	0.22	3.67	3.43	2.61	0.16	72.77	0.3125	0.0058	0.571	0.090
	246.9	0.635	0.624	1.09	0.18	2.79	2.47	1.88	0.14	99.60	0.4278	0.0098	0.581	0.104
	49.6	0.641	0.623	1.09	0.20	2.84	2.29	1.74	0.18	171.16	0.7351	0.0133	0.625	0.132
	4.7	0.238	0.210	0.37	0.08	3.93	3.11	2.36	0.09	255.90	1.0991	0.0186	0.155	0.033
13	5330.4	2.093	1.880	3.28	0.24	8.69	8.62	6.56	6.56	22.79	0.0979	0.0017	0.501	0.039
41.38°N	5263.1	2.421	2.178	3.80	0.26	12.66	12.55	9.55	9.55	33.12	0.1422	0.0022	0.398	0.028
13.89°W	5194.3	2.751	2.747	4.80	0.24	15.80	15.67	11.92	11.92	39.61	0.1701	0.0033	0.403	0.023
	4903.9	2.013	2.009	3.51	0.15	14.79	14.68	11.17	11.17	35.27	0.1515	0.0031	0.314	0.016
	4417.8	2.627	2.624	4.58	0.24	11.16	11.07	8.42	8.42	28.70	0.1233	0.0026	0.545	0.033
	3444	2.399	2.396	4.19	0.14	8.15	8.08	6.14	6.14	22.33	0.0959	0.0022	0.681	0.031
	2464.7	1.569	1.565	2.73	0.26	5.77	5.67	4.31	4.31	30.57	0.1313	0.0028	0.634	0.066
	1187.3	0.869	0.865	1.51	0.12	3.24	3.12	2.38	2.38	37.16	0.1596	0.0032	0.637	0.065
	989.1	1.239	1.234	2.16	0.15	4.16	4.03	3.06	3.06	41.38	0.1777	0.0035	0.704	0.063
	248.4	0.602	0.602	1.05	0.11									
	148.5	0.525	0.525	0.92	0.13									
	29.7	0.508	0.507	0.89	0.11	0.44	0.43	0.32	0.15	5.60	0.0241	0.0015	2.736	1.315
	4.3	0.330	0.330	0.58	0.08	0.28	0.26	0.19	0.14	6.70	0.0288	0.0014	2.968	2.154

Station	Depth	^{231}Pa	^{231}Pa	^{231}Pa$_{corr}$	2se	^{230}Th	^{230}Th	^{230}Th$_{corr}$	2se	^{232}Th	^{232}Th	2se	^{231}Pa/^{230}Th	2se
	m	fg/kg	fg/kg	µBq/kg		fg/kg	fg/kg	µBq/kg		pg/kg	pmol/kg			
21	4514.9	2.605	2.603	4.55	0.15	6.09	6.03	4.58	0.19	20.99	0.0902	0.0017	0.992	0.052
46.54°N	4475	2.404	2.401	4.20	0.18	6.21	6.13	4.66	0.28	25.11	0.1079	0.0025	0.900	0.066
19.67°W	4426.3	2.413	2.411	4.21	0.17	5.76	5.70	4.33	0.14	19.57	0.0841	0.0017	0.972	0.051
	4279.6	2.497	2.495	4.36	0.18	5.91	5.85	4.45	0.19	20.48	0.0880	0.0018	0.980	0.059
	3929.3	2.081	2.079	3.63	0.17	5.47	5.41	4.11	0.16	20.11	0.0864	0.0016	0.884	0.053
	3443.3	1.930	1.928	3.37	0.20	4.63	4.57	3.47	0.14	18.16	0.0780	0.0015	0.970	0.070
	2268.9	1.114	1.114	1.95	0.22	5.16	5.06	3.85	0.17	30.49	0.1309	0.0021	0.506	0.060
	1482.7	0.995	0.993	1.73	0.12	2.48	2.39	1.82	0.14	26.83	0.1152	0.0016	0.953	0.097
	788.4	0.873	0.871	1.52	0.14	1.31	1.23	0.93	0.16	25.41	0.1092	0.0018	1.628	0.312
	445.5	0.679	0.676	1.18	0.14	2.18	2.05	1.56	0.14	39.91	0.1714	0.0023	0.756	0.115
	246.9	0.595	0.592	1.03	0.11	1.64	1.53	1.17	0.13	33.41	0.1435	0.0019	0.886	0.139
	98.1	0.607	0.603	1.05	0.14	1.32	1.23	0.93	0.12	28.01	0.1203	0.0019	1.129	0.209
	13.9	0.536	0.532	0.93	0.15					10.81	0.0464	0.0015		
	3.7	0.522	0.519	0.91	0.14					7.95	0.0342	0.0014		
26	4116.3	1.162	1.158	2.02	0.18	3.43	3.29	2.50	0.17	42.15	0.1810	0.0035	0.808	0.088
50.28°N	2758.5	0.813	0.807	1.41	0.15	3.04	2.85	2.17	0.14	57.40	0.2465	0.0047	0.650	0.081
22.60°W	1973.5	0.745	0.739	1.29	0.13	2.83	2.65	2.01	0.16	56.40	0.2422	0.0045	0.642	0.081
	989.1	0.695	0.695	1.22	0.11									
	296.7	0.503	0.503	0.88	0.10									
	74.4	0.408	0.407	0.71	0.12	0.67	0.62	0.47	0.17	13.57	0.0583	0.0018	1.498	0.603

Station	Depth	^{231}Pa	^{231}Pa	^{231}Pa$_{corr}$	2se	^{230}Th	^{230}Th	^{230}Th$_{corr}$	2se	^{232}Th	^{232}Th	2se	^{231}Pa/^{230}Th	2se
	m	fg/kg	fg/kg	µBq/kg		fg/kg	fg/kg	µBq/kg		pg/kg	pmol/kg			
32	3218.7	0.973	0.968	1.69	0.15	5.49	5.35	4.07	0.15	43.48	0.1867	0.0023	0.416	0.039
55.51°N	3218.5	0.984	0.982	1.72	0.12	1.68	1.63	1.24	0.14	15.25	0.0655	0.0016	1.387	0.184
26.71°W	3049.9	1.131	1.129	1.97	0.11	3.27	3.21	2.44	0.13	20.44	0.0878	0.0016	0.809	0.063
	2949.6	1.076	1.075	1.88	0.17	1.74	1.70	1.29	0.13	12.96	0.0557	0.0014	1.456	0.198
	2854.3	1.004	1.002	1.75	0.20	2.65	2.60	1.97	0.17	16.46	0.0707	0.0016	0.887	0.128
	2610.4	1.109	1.108	1.94	0.13	1.82	1.78	1.35	0.14	12.01	0.0516	0.0016	1.429	0.179
	2218.8	0.843	0.842	1.47	0.14	1.30	1.26	0.96	0.13	11.46	0.0492	0.0015	1.533	0.261
	1676.9	1.200	1.199	2.09	0.14	0.87	0.84	0.64	0.12	9.00	0.0387	0.0014	3.261	0.661
	1185.5	1.087	1.082	1.89	0.14	3.58	3.45	2.62	0.15	40.46	0.1738	0.0022	0.721	0.066
	890.5	0.872	0.869	1.52	0.14	1.64	1.55	1.18	0.13	29.00	0.1246	0.0018	1.289	0.187
	445.3	0.944	0.939	1.64	0.14	2.91	2.76	2.10	0.15	46.20	0.1984	0.0026	0.781	0.086
	222.9	0.568	0.564	0.99	0.12	1.70	1.57	1.20	0.13	39.69	0.1705	0.0022	0.824	0.135
	98.9	0.553	0.550	0.96	0.25	6.65	6.56	4.99	0.16	27.70	0.1190	0.0018	0.193	0.050
	29.5	0.613	0.610	1.07	0.27	5.50	5.41	4.12	0.16	27.73	0.1191	0.0019	0.259	0.067
	5.8	0.584	0.583	1.02	0.14					9.92	0.0426	0.0015		
38	1338.1	1.604	1.602	2.80	0.22	1.62	1.57	1.20	0.15	16.07	0.0690	0.0020	2.341	0.338
58.84°N	1303.6	1.336	1.333	2.33	0.11	3.34	3.25	2.47	0.20	29.18	0.1253	0.0026	0.943	0.087
31.27°W	1234.5	1.088	1.085	1.90	0.11	3.42	3.33	2.53	0.15	28.39	0.1219	0.0026	0.748	0.064
	1084	0.863	0.860	1.50	0.10	3.64	3.54	2.69	0.19	31.67	0.1360	0.0027	0.558	0.053
	494.2	1.621	1.616	2.82	0.25	3.16	3.03	2.30	0.16	39.87	0.1712	0.0033	1.226	0.137
	198.4	1.258	1.253	2.19	0.12	3.12	2.97	2.26	0.14	46.64	0.2003	0.0037	0.969	0.081
	108.7	1.274	1.269	2.22	0.19	2.78	2.65	2.01	0.14	42.89	0.1842	0.0036	1.102	0.121
	20.3	0.836	0.835	1.46	0.13	0.84	0.80	0.61	0.13	11.88	0.0510	0.0016	2.389	0.566
	5.3	1.230	1.228	2.15	0.25	0.80	0.76	0.58	0.15	11.59	0.0498	0.0016	3.719	1.055

Station	Depth	^{231}Pa	^{231}Pa	^{231}Pa$_{corr}$	2se	^{230}Th	^{230}Th	^{230}Th$_{corr}$	2se	^{232}Th	^{232}Th	2se	^{231}Pa/^{230}Th	2se
	m	fg/kg	fg/kg	µBq/kg		fg/kg	fg/kg	µBq/kg		pg/kg	pmol/kg			
44	2918.9	0.839	0.837	1.46	0.17	2.40	2.33	1.77	0.13	22.85	0.0981	0.0022	0.827	0.112
59.62°N	2878.5	0.875	0.873	1.52	0.15	2.50	2.42	1.84	0.14	24.44	0.1050	0.0023	0.829	0.102
38.95°W	2829	0.723	0.723	1.26	0.22									
	2681.9	0.651	0.649	1.13	0.24	2.65	2.57	1.96	0.15	25.27	0.1085	0.0024	0.580	0.129
	2561	1.164	1.161	2.03	0.23	4.87	4.78	3.64	0.17	26.47	0.1137	0.0025	0.557	0.069
	2216.6	0.910	0.906	1.58	0.26	6.18	6.08	4.63	0.18	31.25	0.1342	0.0028	0.342	0.058
	1776	1.416	1.412	2.47	0.39	5.87	5.75	4.37	0.15	39.66	0.1704	0.0032	0.564	0.090
	1382.5	1.186	1.182	2.07	0.27	5.85	5.72	4.35	0.15	41.00	0.1761	0.0034	0.475	0.065
	1087.5	0.795	0.790	1.38	0.18	3.83	3.70	2.81	0.15	40.73	0.1749	0.0033	0.491	0.071
	593.2	1.116	1.111	1.94	0.36	4.28	4.13	3.14	0.16	46.81	0.2010	0.0038	0.618	0.118
	297.3	1.083	1.078	1.88	0.20	4.10	3.97	3.02	0.22	42.29	0.1816	0.0036	0.625	0.081
	78.8	0.929	0.925	1.62	0.19	3.44	3.31	2.52	0.14	39.69	0.1705	0.0033	0.641	0.082
	25.5	0.998	0.997	1.74	0.16	1.37	1.32	1.00	0.15	16.50	0.0709	0.0019	1.737	0.297
	5.5	0.722	0.720	1.26	0.33	1.31	1.27	0.96	0.12	14.99	0.0644	0.0018	1.307	0.380
60	1710.9	0.844	0.841	1.47	0.07	3.77	3.67	2.79	0.16	31.42	0.1349	0.0031	0.526	0.039
59.80°N	1652.6	0.881	0.878	1.53	0.07	4.03	3.92	2.98	0.16	33.28	0.1429	0.0032	0.514	0.036
42.01°W	1603.1	0.845	0.842	1.47	0.07	4.10	3.99	3.04	0.24	33.74	0.1449	0.0032	0.485	0.045
	1481.2	0.813	0.809	1.41	0.07	4.19	4.08	3.10	0.17	33.94	0.1458	0.0032	0.455	0.034
	989.7	1.087	1.082	1.89	0.08	5.29	5.15	3.91	0.20	45.60	0.1958	0.0040	0.483	0.031
	495.5	0.911	0.906	1.58	0.16	3.69	3.56	2.71	0.14	39.63	0.1702	0.0033	0.585	0.064
	247.9	0.851	0.847	1.48	0.23	3.16	3.03	2.30	0.14	40.61	0.1744	0.0034	0.643	0.109
	99.1	0.826	0.822	1.44	0.20	2.34	2.23	1.69	0.13	34.75	0.1492	0.0029	0.849	0.134
	19.5	0.887	0.885	1.55	0.32	1.36	1.30	0.99	0.16	18.14	0.0779	0.0020	1.561	0.405
	3.7	0.829	0.827	1.44	0.24	1.53	1.46	1.11	0.14	22.32	0.0959	0.0023	1.301	0.266

Station	Depth	^{231}Pa	^{231}Pa	^{231}Pa$_{corr}$	2se	^{230}Th	^{230}Th	^{230}Th$_{corr}$	2se	^{232}Th	^{232}Th	2se	^{231}Pa/^{230}Th	2se
	m	fg/kg	fg/kg	µBq/kg		fg/kg	fg/kg	µBq/kg		pg/kg	pmol/kg			
64	2466.8	0.759	0.756	1.32	0.19	3.24	3.16	2.40	0.14	25.71	0.1104	0.0025	0.551	0.087
59.07ºN	2423.6	0.828	0.825	1.44	0.20	3.71	3.62	2.76	0.18	26.12	0.1122	0.0027	0.523	0.080
46.08ºW	2374	0.958	0.955	1.67	0.19	3.76	3.68	2.80	0.13	27.16	0.1166	0.0025	0.597	0.074
	2226.6	1.051	1.048	1.83	0.27	5.33	5.24	3.99	0.15	29.28	0.1257	0.0028	0.460	0.070
	1775.6	1.155	1.152	2.01	0.20	5.50	5.38	4.10	0.17	34.64	0.1488	0.0038	0.491	0.054
	890	1.112	1.106	1.93	0.19	4.56	4.39	3.34	0.19	53.17	0.2283	0.0045	0.579	0.066
	395.2	0.898	0.894	1.56	0.17	3.61	3.48	2.65	0.18	40.79	0.1752	0.0110	0.590	0.074
	247.4	0.923	0.918	1.60	0.26	3.23	3.10	2.36	0.18	40.00	0.1718	0.0038	0.680	0.122
	99.2	1.044	1.039	1.81	0.23	3.45	3.30	2.51	0.16	46.12	0.1981	0.0041	0.723	0.105
	29.5	0.963	0.960	1.68	0.28	2.18	2.08	1.58	0.14	30.23	0.1298	0.0029	1.060	0.200
	5.1	0.768	0.766	1.34	0.21	1.54	1.46	1.11	0.17	23.73	0.1019	0.0024	1.202	0.269
69	3676.5	0.404	0.402	0.70	0.10	1.94	1.88	1.43	0.21	19.60	0.0842	0.0025	0.491	0.099
55.84ºN	3637.3	0.336	0.334	0.58	0.12	1.92	1.86	1.41	0.16	19.15	0.0822	0.0023	0.414	0.098
48.09ºW	3589.5	0.438	0.436	0.76	0.11	2.15	2.08	1.58	0.19	21.39	0.0919	0.0024	0.482	0.091
	3444.7	0.528	0.525	0.92	0.11	3.58	3.49	2.65	0.19	27.76	0.1192	0.0028	0.346	0.048
	2951.8	0.581	0.578	1.01	0.11	5.75	5.64	4.29	0.23	33.80	0.1452	0.0032	0.235	0.029
	2462.6	0.604	0.599	1.05	0.11	6.44	6.31	4.80	0.21	39.48	0.1696	0.0037	0.218	0.025
	2168.1	0.855	0.850	1.49	0.12	6.03	5.90	4.49	0.22	40.95	0.1759	0.0039	0.331	0.031
	1481.3	0.670	0.661	1.16	0.10	4.98	4.73	3.60	0.20	79.22	0.3402	0.0066	0.321	0.033
	989	0.729	0.723	1.26	0.11	4.53	4.35	3.31	0.21	57.18	0.2456	0.0049	0.382	0.041
	445.6	0.692	0.686	1.20	0.07	4.23	4.05	3.08	0.23	55.48	0.2383	0.0047	0.389	0.037
	248.8	0.604	0.598	1.04	0.07	4.06	3.87	2.95	0.18	59.43	0.2552	0.0052	0.355	0.033
	99.5	0.513	0.507	0.89	0.10	3.58	3.40	2.58	0.22	56.06	0.2408	0.0049	0.343	0.047
	28.7	0.554	0.550	0.96	0.07	1.50	1.40	1.07	0.24	30.11	0.1293	0.0029	0.903	0.210
	8.2	0.457	0.453	0.79	0.07	1.42	1.31	0.99	0.17	34.28	0.1472	0.0031	0.797	0.153

Station	Depth	^{231}Pa	^{231}Pa	^{231}Pa$_{corr}$	2se	^{230}Th	^{230}Th	^{230}Th$_{corr}$	2se	^{232}Th	^{232}Th	2se	^{231}Pa/^{230}Th	2se
	m	fg/kg	fg/kg	µBq/kg		fg/kg	fg/kg	µBq/kg		pg/kg	pmol/kg			
77	2487.5					4.02	3.93	2.99	0.14	29.43	0.1264	0.0026		
53°N	2462.8	1.261	1.258	2.20	0.15	4.07	3.97	3.02	0.14	30.06	0.1291	0.0026	0.728	0.059
51.10°W	2414.2	1.113	1.110	1.94	0.10	4.09	4.00	3.04	0.15	29.56	0.1270	0.0026	0.638	0.044
	2268.5	0.989	0.985	1.72	0.12	6.11	6.00	4.56	0.16	33.99	0.1460	0.0030	0.377	0.029
	2170.5	1.355	1.352	2.36	0.13	5.32	5.22	3.97	0.17	30.77	0.1322	0.0028	0.595	0.041
	1678.1	1.267	1.263	2.21	0.13	5.48	5.36	4.08	0.16	37.02	0.1590	0.0031	0.541	0.039
	1235.4	0.580	0.576	1.01	0.13	5.36	5.22	3.97	0.18	44.75	0.1922	0.0037	0.253	0.035
	989.6	1.772	1.767	3.09	0.23	4.96	4.79	3.64	0.17	53.23	0.2286	0.0041	0.848	0.073
	496.4					4.33	4.15	3.16	0.17	55.68	0.2391	0.0044		
	297.9	0.501	0.494	0.86	0.07	4.71	4.50	3.42	0.23	64.41	0.2766	0.0055	0.252	0.026
	78.8	1.200	1.193	2.08	0.14	3.50	3.29	2.50	0.20	65.47	0.2812	0.0053	0.834	0.086
	2.5	0.926	0.923	1.61	0.12	1.34	1.25	0.95	0.17	28.01	0.1203	0.0026	1.699	0.332

^{230}Th and ^{231}Pa are dissolved ^{230}Th and ^{231}Pa activities corrected for the ingrowth from seawater ^{234}U and ^{235}U, respectively, since the time of collection following equations:

$$^{230}Th = {}^{230}Th_m - {}^{234}U \times \left(1 - \exp\left(-\lambda_{^{230}Th} \times t\right)\right) \quad (1)$$

$$^{231}Pa = {}^{231}Pa_m - {}^{235}U \times \left(1 - \exp\left(-\lambda_{^{231}Pa} \times t\right)\right) \quad (2)$$

^{230}Th and ^{231}Pa are further corrected for detrital, U-supported ^{230}Th and ^{231}Pa concentrations as follows:

$$^{230}Th_{corr} = {}^{230}Th_m - (0.6 \times {}^{232}Th_m) \quad (3)$$

$$^{231}Pa_{corr} = {}^{231}Pa_m - 0.046 \times (0.6 \times {}^{232}Th_m) \quad (4)$$

where ^{230}Th$_m$, ^{231}Pa$_m$ and ^{232}Th$_m$ are activities obtained from measurement; ^{235}U and ^{234}U are their average activities in seawater, 1824 µBq/kg (112 dpm/1000l) and 45551µBq/kg (2801 dpm/1000l,) respectively, obtained from ^{238}U activity of 39610 µBq/kg (2436 dpm/1000l) at salinity of 35 (Owens et al., 2011) and assuming natural ^{238}U/^{235}U abundance ratio of 137.88 and seawater ^{234}U/^{238}U activity ratio of 1.15; $\lambda_{^{230}Th}$ and $\lambda_{^{231}Pa}$ are decay constants of ^{230}Th and ^{231}Pa; t is the time between sample collection and chemical separation of U from ^{231}Pa and ^{230}Th. 0.6 is the average ^{238}U/^{232}Th activity ratio in detrital material in the Atlantic (Henderson and Anderson, 2003) and 0.046 represents ^{235}U/^{238}U activity ratio in seawater (Anderson et al., 1990). Half-lives for ^{231}Pa, ^{230}Th and ^{232}Th are 32,760 yr, 75,584 yr and 1.40×10^{10} yr (Cheng et al., 2013; Holden, 1990; Robert et al., 1969).

All errors are two standard errors (2se) and include the contribution from sample weighing, spike calibration, ^{231}Pa, ^{230}Th and ^{232}Th in the respective ^{233}Pa and ^{230}Th spikes, blank correction, internal precision and related corrections of mass spectrometric measurement.

S2. CFC-based Age determination

CFC measurement are not available for the GEOVIDE cruise itself. However, with the availability of CFC measurements from OVIDE section in 2012 and water mass composition estimated using extended Optimum Multi-Parameter (eOMP) analysis for both OVIDE and GEOVIDE sections, CFC-based ages can be derived for GEOVIDE section.

1. CFC measurements were available along OVIDE section in 2012 (OVIDE/CATARINA cruise) (de la Paz et al., 2017). This allows the computing of the mean age of water masses using transient time distribution (TTD) method. A more detailed description of TTD method is given in other studies (e.g. Steinfeldt et al., 2009; Waugh et al., 2003). It is important to note that this mean age (referred to as CFC-based age hereafter and in the manuscript) is different from the age calculated based on atmospheric history of CFC (referred to as CFC apparent age hereafter), and therefore is not limited by the time span of the presence of CFC in the atmosphere and inherently deals with age bias due to water mass mixing in CFC apparent age.

Combining CFC-based ages computed with the TTD method for each water sample with water mass composition estimated using eOMP analysis for OVIDE section in 2012 (García-Ibáñez et al., 2015), CFC-based age was calculated for each Source Water Type (SWT) defined in García-Ibáñez et al., 2015 by the equations,

$$\log\,[\text{CFC–based age}]^j = \sum_{i=1}^{12} SWT_i^j \times (log[\text{CFC–based age}]_i) + \varepsilon_j \; j = 1 \rightarrow 424 \; samples \quad (5)$$

$$[\text{CFC} - \text{Age}]^j = \text{anti}\log\,[\text{CFC} - \text{Age}]^j \; (6)$$

where SWT_i^j is the fraction of SWT *"i"* to sample *"j"* (obtained through the eOMP analysis); $[\text{CFC–based age}]^j$ is CFC-based age for each water sample computed with TTD method along OVIDE section 2012; and ε_j is the residual, representing the portion of CFC–based age that can not be modelled by mixing of SWTs, i.e. the difference between $\log\,[\text{CFC–based age}]^j$ and that obtained as the sum of the contributions by mixing of the individual SWT, $\sum_{i=1}^{12} SWT_i^j \times (log[\text{CFC–based age}]_i)$.

The output of $\log[\text{CFC-based age}]_i$ and its inversion ($[\text{CFC-age}]_i$) is given in Table S2. The squared correlation coefficient (r^2) and standard deviation of the residual, ε_j, are 0.94 and 0.12, respectively.

2. CFC-based age for GEOVIDE section was then calculated employing equation (5) with water mass composition estimated using eOMP analysis along GEOVIDE section (García-Ibáñez et al., 2018) and the output of CFC-based age for SWT (Table S2).

Table S2 Output of log(CFC-age) and the inversion [CFC-age]$_I$ (i.e. CFC-based age) for source water types (SWT)

	log(CFC-age)	CFC-based age
ENACW$_{16}$	1.05±0.20	11±5
ENACW$_{12}$	1.11±0.03	13±1
SPMW$_8$	1.69±0.04	49±5
SAIW	1.19±0.07	16±3
SPMW$_7$	1.26±0.05	18±2
IrSPMW	0.98±0.03	10±1
LSW	1.54±0.02	35±1
MW	1.96±0.04	91±8
PIW	1.33±0.15	22±8
DSOW	1.22±0.07	17±3
ISOW	1.70±0.03	50±4
NEADW$_L$	3.00±0.02	989±48
r^2	0.94	0.943
std(Resid)	0.12	41

ENACW$_{16}$ and ENACW$_{12}$ = East North Atlantic Central Water of 16ºC and 12ºC; SPMW$_8$, SPMW$_7$, IrSPMW = Subpolar Mode Water of 8ºC, 7ºC and of the Irminger Sea; SAIW = Subarctic Intermediate Water; MW = Mediterranean Water; PIW = Polar Intermediate Water; ISOW=Iceland–Scotland Overflow Water; LSW=Labrador Sea Water; DSOW: Denmark Strait Overflow Waters; and NEADW$_L$: Lower North East Atlantic Deep Water. r^2 and std (Resid) represents the squared correlation coefficient and standard deviation of the residual, ε_j, i.e. the difference between log [CFC–based age]^j and that obtained as the sum of the contributions by mixing of the individual SWT, $\sum_{i=1}^{12} SWT_i^j \times (log[\text{CFC–based age}]_i)$.

S3. Scavenging-mixing model and parameterization

A more detailed description of the scavenging-mixing model used in this this study is given in Moran et al. (1997). Briefly, the model takes into account reversible scavenging of the nuclides and water mass mixing. It describes the evolution of nuclides through time in a one-dimensional system, an ocean water column. In the Atlantic, the system is assumed to start at time t=0 in the far North Atlantic and moves southward with time. Transport of material downward relative to the direction of water flow is permitted, to represent the effect of scavenging of radionuclides by sinking particles. Lateral exchange with water outside of the system is not permitted.

The equations to derive the dissolved concentration of each nuclide follows those of Moran et al., (1997). Dissolved concentration of the nuclide is given by,

$$c_d = \frac{C_{pre,t} + P \quad \tau_w}{(K_d\ SPM+1)} \times [1 - \exp(-\frac{(K_d\ SPM+1)}{SK_d\ \tau_w SPM} \times z)] \quad (7)$$

where C_d is the dissolved concentration of the nuclide ; P is the production rate of ^{230}Th and ^{231}Pa, 0.42 µBq/kg/yr (2.57 × 10^{-2} dpm/1000l/yr) and 0.039 µBq/kg/yr (2.37 × 10^{-3} dpm/1000l/yr), respectively; K_d is the distribution coefficient of the nuclide; λ is the decay constant of the nuclide; $C_{pre,t}$ is the preformed total concentration of ^{230}Th (or ^{231}Pa); SPM is the suspended particle concentration; and S is the particle settling speed, which represents the net effect of particle sinking, disaggregation and aggregation; τ_w is water mass age; z is the water depth.

Initial parameterization was conducted using S=500-1000 m/yr, K_d^{Th}= 1× 10^7 ml/g, K_d^{Pa}= 5× 10^5 ml/g, SPM= 20-50 µg/l, for preformed concentrations set at 0 and surface average from GEOVIDE, i.e., $C_{pre}^{Th} = C_{surface\ average}^{Th}$ = 1.66 µBq/kg, $C_{pre}^{Pa} = C_{surface\ average}^{Pa}$ = 1.31 µBq/kg. With τ_w known from CFC measurements for every depth where ^{230}Th and ^{231}Pa was measured along GEOVIDE section, water-column profiles of both nuclides were simulated for GEOVIDE Station 13 and the parameters were adjusted for the best fit between the simulated and observed profiles (Fig. S1). This gives us the optimized parameters for the analysis in discussion section 4.3, which are listed in Table S3. Our optimized parameters are consistent with values reported by other studies (also listed in Table S3).

Adopting the optimized parameters and setting preformed component (C_{pre}) equal to the nuclide concentrations observed in the upper 100 m of the GEOVIDE section, the modelled evolution of nuclide concentrations with age between 0-500 years at 2000 m and 3500 m water depths, together with GEOVIDE data, is plotted in Figure S2.

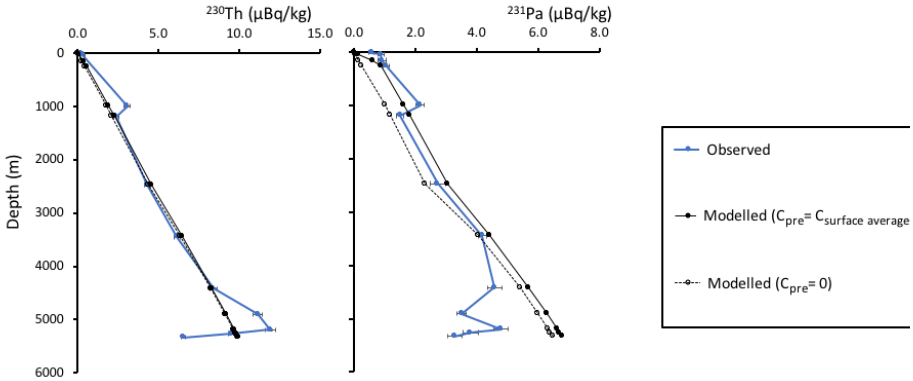

Figure S1: Modelled (dashed black lines) profiles with preformed value set at 0 and surface average concentration from GEOVIDE, and observed (solid blue lines) profiles of Station 13 from GEOVIDE section. The best fit was first sought for ^{230}Th, which gives us the optimized parameters S, SPM and K_d^{Th}. These parameters were then adopted for the simulation of ^{231}Pa profiles, adjusting only K_d^{Pa} to obtain the best fit.

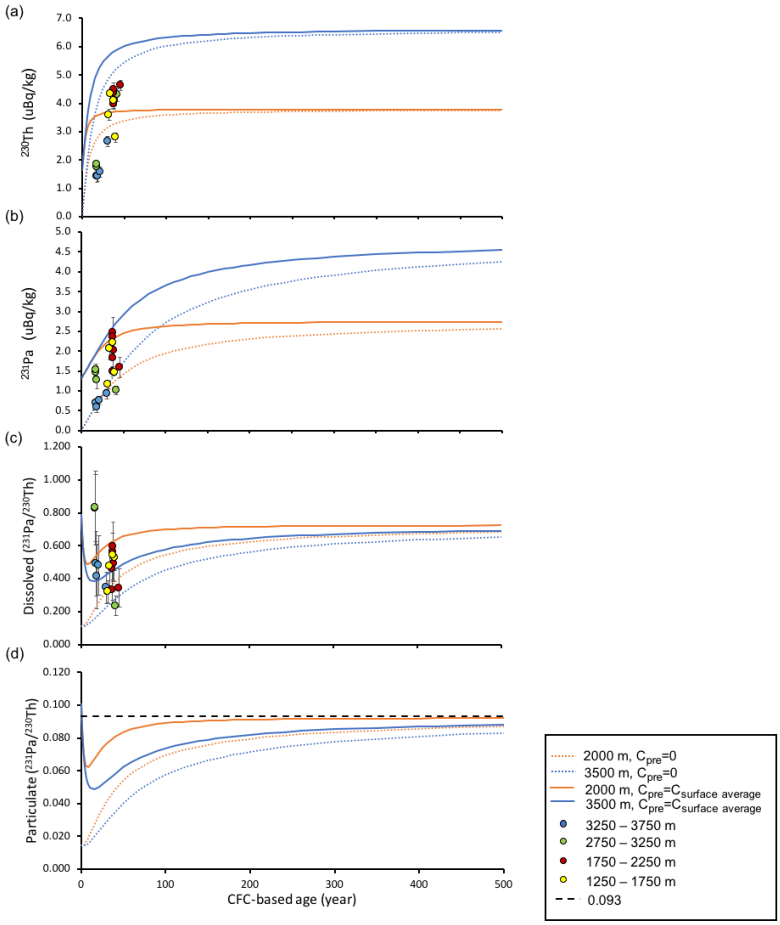

Figure S2: Results from a scavenging-mixing model of ^{230}Th, ^{231}Pa, Dissolved ^{231}Pa/^{230}Th and Particulate ^{231}Pa/^{230}Th compared to observations. Preformed concentration (C_{pre}) were set at 0 (dashed line) and at the average surface concentration ($C_{surface\ average}$) from GEOVIDE section (solid line), i.e. ^{230}Th= 1.66 µBq/kg, ^{231}Pa= 1.31 µBq/kg.

Table S3 Parameterization of the scavenging-mixing model

	This study	Literature
S (m/yr)	800	500-1000 (Moran et al., 1997)
SPM (μg/l)	25	30 (Labrador Sea, Brewer et al., 1976)
K_d^{Th} (ml/g)	1.1×10^7	1.1×10^7 (Moran et al., 1997)
K_d^{Pa} (ml/g)	1.4×10^6	2.2×10^5 (pure carbonate)~1.4×10^6 g/g (pure opal) (pseudo-K_d, Chase et al., 2002)

S4. Meridional transport of ^{230}Th and ^{231}Pa in the Atlantic

Table S4 Mass balance calculation of meridional transport of ^{230}Th and ^{231}Pa in the Atlantic

	Net meridional transport		Volume of seawater between two latitudes	Production in water column		Removal to sediment		Removal/Production	
	$\times 10^{10}$ μBq/s		$\times 10^{17}$ m^3	$\times 10^{10}$ μBq/s		$\times 10^{10}$ μBq/s		%	
	^{230}Th	^{231}Pa		^{230}Th	^{231}Pa	^{230}Th	^{231}Pa	^{230}Th	^{231}Pa
GEOVIDE-4.5°S	-7.76	-4.75	1.48	200.8	18.6	193.1	13.8	96.2	74.2
4.5°S-45°S	0.33	0.017	1.02	138.4	12.8	138.7	12.8	99.8	100.0

Positive value indicates northward transport; negative value indicates southward transport. Production rate of ^{230}Th and ^{231}Pa in water column are 0.42 and 0.039 μBq/kg/yr, respectively.

References

Anderson, R. F., Lao, Y., Broecker, W. S., Trumbore, S. E., Hofmann, H. J. and Wolfli, W.: Boundary scavenging in the Pacific Ocean: a comparison of ^{10}Be and ^{231}Pa, Earth Planet. Sci. Lett., 96(3), 287–304, doi:https://doi.org/10.1016/0012-821X(90)90008-L, 1990.

Brewer, P. G., Spencer, D. W., Biscaye, P. E., Hanley, A., Sachs, P. L., Smith, C. L., Kadar, S. and Fredericks, J.: The distribution of particulate matter in the Atlantic Ocean, Earth Planet. Sci. Lett., 32(2), 393–402, doi:https://doi.org/10.1016/0012-821X(76)90080-7, 1976.

Chase, Z., Anderson, R. F., Fleisher, M. Q. and Kubik, P. W.: The influence of particle composition and particle flux on

Deleted: ¶

S4. Uncertainty analysis of the assessment of the scavenging of ^{230}Th and ^{231}Pa¶

Both the uncertainty of the CFC-based ages an the fact that the preformed values of ^{230}Th and ^{231}Pa are unknown contribute to the uncertainty of the scavenging of ^{230}Th and ^{231}Pa. Here we analyze how these two factors influence the assessment of the scavenging of ^{230}Th and ^{231}Pa.¶

1. CFC-based ages¶

Uncertainties (1 standard error) associated with CFC-based age range between 11-40%. This uncertainty leads to an average uncertainty of 23% and 13% in potential total ^{230}Th and ^{231}Pa respectively, corresponding to an average uncertainty of 30% in the scavenged component of ^{230}Th and 40% in the scavenged component of ^{231}Pa. ¶

2. Preformed values¶

As the exact values of preformed values are unknown, we analyse the sensitivity of the scavenging component to this factor. A two-fold increase in preformed values results in an increase by a factor of 1.2 and 1.6 in the total potential component of ^{230}Th and ^{231}Pa, respectively, leading to an increase by a factor of 1.2 in the scavenged component of ^{230}Th and of 2.6 in the scavenged component of ^{231}Pa. Clearly, the scavenged component of ^{231}Pa is more sensitive to the preformed component compared with the scavenged component of ^{230}Th. This difference however becomes less significant when comparing the scavenging component to the potential total component, i.e. the ratio of scavenged/potential total, with an increase in the ratio of scavenged/potential total by a factor of 1.1 and 1.4 for ^{230}Th and ^{231}Pa, respectively. This sensitivity analysis suggests that a better knowledge of preformed values will benefit the assessment of the scavenging of both nuclides. ¶

Deleted: 5

Deleted: ¶

¶

Formatted: Superscript

Formatted: Superscript

Deleted: a

scavenging of Th, Pa and Be in the ocean, Earth Planet. Sci. Lett., 204(1), 215–229, doi:https://doi.org/10.1016/S0012-821X(02)00984-6, 2002.

Cheng, H., Lawrence Edwards, R., Shen, C.-C., Polyak, V. J., Asmerom, Y., Woodhead, J., Hellstrom, J., Wang, Y., Kong, X., Spötl, C., Wang, X. and Calvin Alexander, E.: Improvements in ^{230}Th dating, ^{230}Th and ^{234}U half-life values, and U–Th isotopic measurements by multi-collector inductively coupled plasma mass spectrometry, Earth Planet. Sci. Lett., 371, 82–91, doi:10.1016/j.epsl.2013.04.006, 2013.

García-Ibáñez, M. I., Pardo, P. C., Carracedo, L. I., Mercier, H., Lherminier, P., Ríos, A. F. and Pérez, F. F.: Structure, transports and transformations of the water masses in the Atlantic Subpolar Gyre, Prog. Oceanogr., 135, 18–36, doi:https://doi.org/10.1016/j.pocean.2015.03.009, 2015.

García-Ibáñez, M. I., Pérez, F. F., Lherminier, P., Zunino, P., Mercier, H. and Tréguer, P.: Water mass distributions and transports for the 2014 GEOVIDE cruise in the North Atlantic, Biogeosciences, 15(7), 2057–2090 [online] Available from: https://doi.org/10.5194/bg-15-2075-2018, 2018.

Henderson, G. M. and Anderson, R. F.: The U-series Toolbox for Paleoceanography, Rev. Mineral. Geochemistry, 52(1), 493–531 [online] Available from: http://dx.doi.org/10.2113/0520493, 2003.

Holden, N. E.: Total half-lives for selected nuclides, Pure Appl. Chem., 62, 941, doi:10.1351/pac199062050941, 1990.

de la Paz, M., García-Ibáñez, M. I., Steinfeldt, R., Ríos, A. F. and Pérez, F. F.: Ventilation versus biology: What is the controlling mechanism of nitrous oxide distribution in the North Atlantic?, Global Biogeochem. Cycles, 31(4), 745–760, doi:10.1002/2016GB005507, 2017.

Moran, S. B., Charette, M. A., Hoff, J. A. and Edwards, R. L.: Distribution of 230Th in the Labrador Sea and its relation to ventilation, Earth Planet. Sci. Lett., 150, 151–160, 1997.

Owens, S. A., Buesseler, K. O. and Sims, K. W. W.: Re-evaluating the 238U-salinity relationship in seawater: Implications for the 238U–234Th disequilibrium method, Mar. Chem., 127(1), 31–39, doi:https://doi.org/10.1016/j.marchem.2011.07.005, 2011.

Robert, J., Miranda, C. F. and Muxart, R.: Mesure de la période du protactinium 231 par microcalorimétrie, Radiochim. Acta, 11(2), 104–108, doi:10.1524/ract.1969.11.2.104, 1969.

Steinfeldt, R., Rhein, M., Bullister, J. L. and Tanhua, T.: Inventory changes in anthropogenic carbon from 1997–2003 in the Atlantic Ocean between 20°S and 65°N, Global Biogeochem. Cycles, 23(3), doi:10.1029/2008GB003311, 2009.

Waugh, D. W., Hall, T. M. and Haine, T. W. N.: Relationships among tracer ages, J. Geophys. Res., 108(C5), 3138, doi:10.1029/2002JC001325, 2003.